JULY 1991

FIELD ANALYSIS ON THE ROLE OF THREE-DIMENSIONAL MOISTURE FLOW IN GROUND-WATER RECHARGE AND EVAPOTRANSPIRATION

Technical Completion Report No. 260

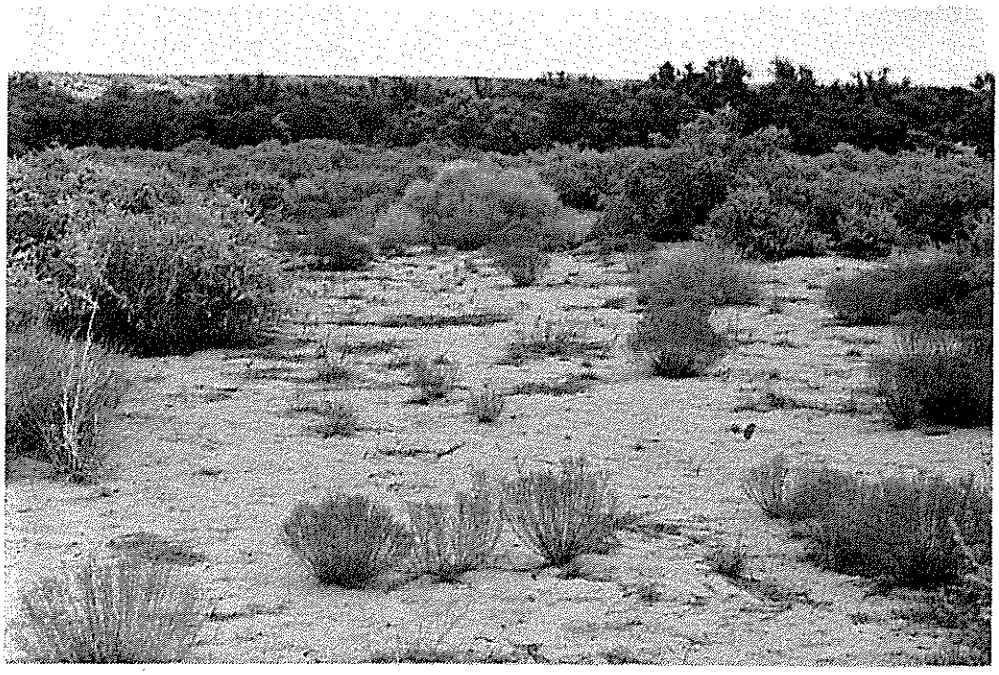

NEW MEXICO WATER RESOURCES RESEARCH INSTITUTE
New Mexico State University
Box 30001, Dept. 3167
Las Cruces, New Mexico 88003-0001
Telephone (505) 646-4337 FAX (505) 646-6418

FIELD ANALYSIS ON THE ROLE OF THREE-DIMENSIONAL MOISTURE FLOW IN GROUND-WATER RECHARGE AND EVAPOTRANSPIRATION

By

Daniel B. Stephens
Principal Investigator
Department of Geoscience
New Mexico Tech

and

Eric Hicks and Todd Stein
Graduate Research Assistants
Department of Geoscience
New Mexico Tech

TECHNICAL COMPLETION REPORT

Project Number 1345669

July 1991

New Mexico Water Resources Research Institute
in Cooperation with
Department of Geoscience, New Mexico Tech

The research on which this report is based was financed in part by the US Department of the Interior, Geological Survey, through the New Mexico Water Resources Research Institute.

DISCLAIMER

The purpose of Water Resources Research Institute technical reports is to provide a timely outlet for research results obtained on projects supported in whole or in part by the institute. Through these reports, we are promoting the free exchange of information and ideas and hope to stimulate thoughtful discussion and action that may lead to resolution of water problems. The WRRI, through peer review of draft reports, attempts to substantiate the accuracy of information contained in its reports, but the views expressed are those of the author(s) or its reviewers.

Contents of this publication do not necessarily reflect the views and policies of the United States Department of the Interior, nor does mention of trade names or commercial products constitute their endorsement by the United States Government.

ABSTRACT

In comparison to evapotranspiration, ground-water recharge is usually a small part of the hydrological cycle in areas of low precipitation; nevertheless, the replenishment of our underground water resources depends upon this important process. A field program was developed to quantify recharge and soil-water flow directions through sandy soil in a desert landscape near Socorro, New Mexico. The instrumentation consisted of two climatological stations and a dense grid work of 160 tensiometers and 12 neutron probe access tubes to monitor pressure head and moisture content located within a 24 m^2 area. The results of measurements from July 1988 to July 1989 showed that soil-water uptake by saltbush and desert shrubs did not induce significant horizontal flow components. We conclude that for this, and similar sites, a one-dimensional analysis of soil-water movement is adequate. Recharge was about 0.4 cm/yr and comprised about 2.3% of the 17.4 cm/yr rainfall.

Keywords: Ground water, Recharge, Evapotranspiration, Infiltration, Arid-Land Hydrology.

TABLE OF CONTENTS

LIST OF FIGURES

LIST OF FIGURES
(continued)

LIST OF TABLES

INTRODUCTION

Ground-water recharge is the process by which water stored in aquifers is replenished. Although in semiarid climates recharge to ground water may be small compared to other components of the hydrologic budget such as evapotranspiration, when one considers vast lowland areas where deep infiltration of precipitation may occur, then the volume of recharge may become very significant indeed, especially with respect to domestic water needs. Quantifying ground-water recharge is the key to managing the long-term yield of aquifers. Therefore, identifying and protecting significant recharge areas becomes an important element of water resources planning, especially in low rainfall areas. An understanding of ground-water recharge and evapotranspiration processes in the hydrologic cycle is highly relevant to improving our ability to optimize the water use in desert ecosystems.

In semiarid areas where mean annual potential evapotranspiration of soil-moisture is much greater than mean annual precipitation, ground-water recharge is considered by some to be virtually nil. However, in a sandy lowland area at the Sevilleta National Wildlife Refuge near Socorro (Figure 1), Stephens and Knowlton (1986) demonstrated that, locally, recharge beneath part of a poorly vegetated desert rangeland may be as much as 20% of the annual precipitation. This occurs even though potential evaporation at this site exceeds precipitation by about a factor of 2 in winter and 14 in summer (Stephens et al. 1985). Similar results were obtained in unvegetated coarse-textured soils near Hanford, Washington where precipitation was about 12 cm/yr (Gee et al. 1989). However, as Gee and Hillel (1988) observed, site-specific recharge often cannot be expressed simply as a percentage of annual precipitation, due to spatial and temporal variability in soil-water flux caused by vegetation, topography, and soil properties. Nevertheless, it is apparent that some storms, or sequences of storms, produce sufficient rainfall to cause moisture to penetrate to depths below which the moisture cannot be quickly evaporated or extracted by roots. Depending upon the storm characteristics, soil moisture status, soil permeability, and atmospheric conditions following the storm, the proportions of any particular precipitation event which become deep percolation or evapotranspiration may vary drastically. In semiarid climates, native vegetation is usually sparse, and the nonuniform plant distribution could lead to significant variations in soil moisture induced by the spatial heterogeneity of plant roots and by the seasonal changes in water demand by the plant.

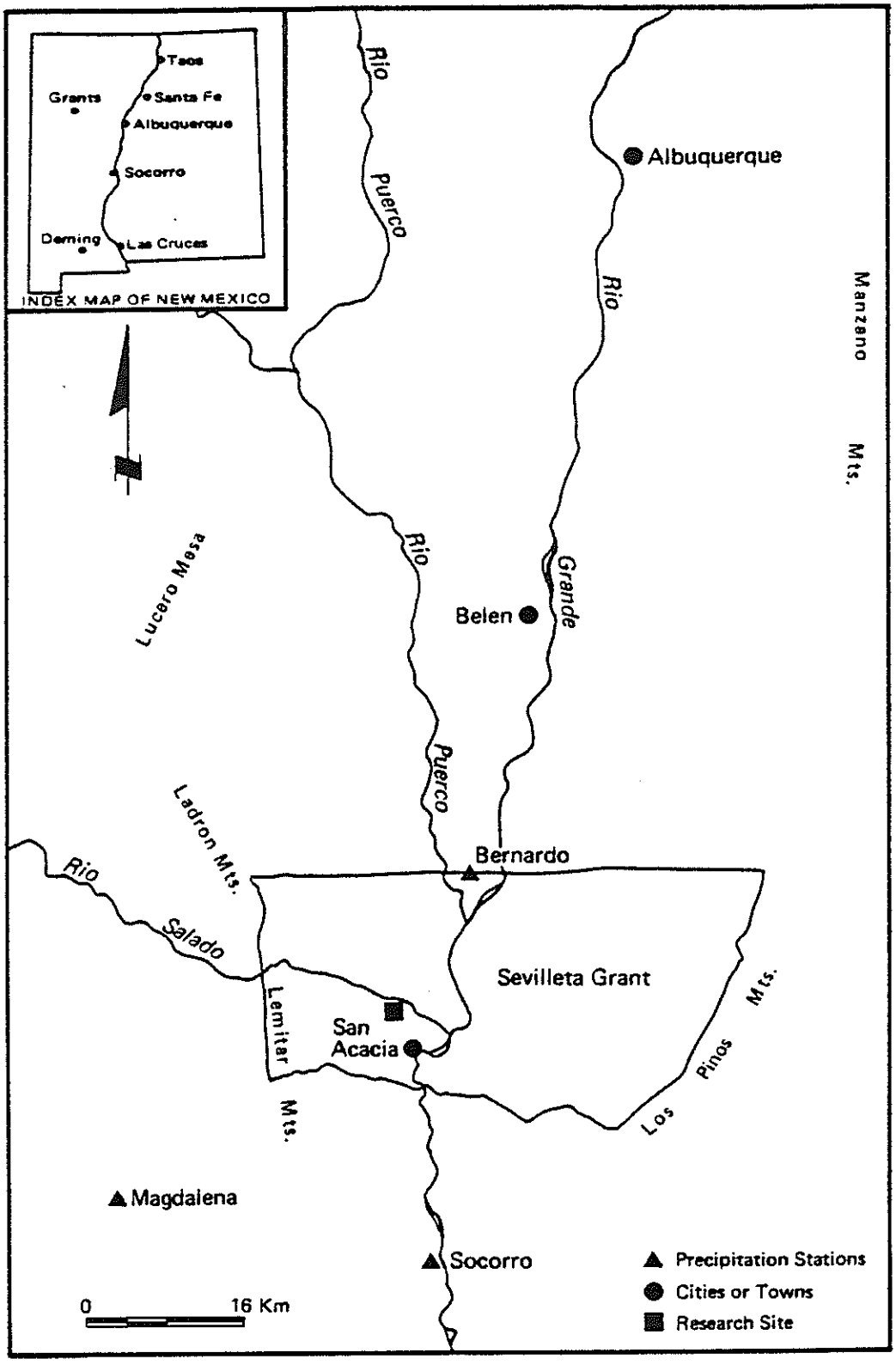

FIGURE 1. Regional site location map.

In light of these potential spatial and temporal variations in soil-water uptake by plants, it is likely that soil-water movement could have a three-dimensional flow component, at least part of the year. The significance of three-dimensional moisture flow near sparse desert shrub communities has not been fully evaluated by researchers to date. Preliminary field evidence (Kickham 1987) suggests that significant errors may occur in commonly used methods to quantify ground-water recharge and evapotranspiration which are based on a one-dimensional flow conceptual model. In addition, some of the evapotranspiration models, which assume that the landscape is fully vegetated and contains uniform root distributions, may also lead to incorrect results. An understanding of the physical controls on soil-water movement at a local scale is essential to developing predictive models at a large scale and to evaluating their inherent deficiencies.

The analysis of natural soil-water movement at the local scale is also relevant to the migration of contaminants spilled on the land surface. In winter when desert plants may be dormant and evapotranspiration rates are low, contaminants may move downward past the root zone toward the water table. On the other hand, in summer, soil moisture which contains dissolved contaminants may migrate laterally toward plant roots. Having information on the duration and effectiveness of such a process could play an important role in remedial action decisions such as excavation of the contaminated soil. During the process of water and contaminant migration through soils, it is also important to recognize that contaminants assimilated by the plants during parts of the year may become concentrated in the food chain.

Objectives of this investigation were:

1. to quantify, to the extent practical, ground-water recharge from in situ soil-moisture data;

2. to investigate the directions of soil-moisture flow in the root zone of desert shrubs;

3. to examine the significance of the horizontal flow components on soil-water movement; and

4. to evaluate the seasonal variability of soil-water movement in a desert plant community.

To accomplish these objectives, we intensively instrumented a plot of uncultivated sandy soil surrounded by native desert vegetation. This site was characterized for geology, hydrologic properties, climatology, and plant root systems. The instrumentation, which included tensiometers and neutron probe access tubes, was monitored for approximately one year to determine the direction and rate of soil-water movement.

SITE DESCRIPTION

The study area is located within the Sevilleta National Wildlife Refuge about 20 km north of Socorro, New Mexico. Previous work in this area on a sand dune, in particular research by graduate students James McCord (1986) and Barbara Kickham (1987), suggested that significant horizontal components to soil-water movement can occur near the land surface in homogeneous sandy soils (Figure 2). Motivated by their findings, we established an extensive data collection network in the fluvial sand facies on the abandoned flood-plain terrace of the Rio Salado (Figure 3), an ephemeral tributary of the Rio Grande. The instrumented site slopes very gently to the north and exhibits no evidence of channelized runoff, owing to the high permeability of the unconsolidated sandy soil.

The study area is situated within the northern part of the Chihuahua desert, a region that extends south along the Rio Grande, into Mexico, and includes parts of west Texas. Precipitation is highly variable in the Chihuahua desert, ranging from 7 to 30 cm annually. Most precipitation comes as brief but intense summer thunderstorms, and as gentle winter rain and snow. Temperatures may range from 40°C in summer to -10°C in winter.

Vegetation in the study area is predominantly creosote bush, four-wing saltbush, indigo bush (purple sage), mesquite, snakeweed, sacatone, annual mustard, and juniper. Grasses and cacti include gramma grass, spectacle pod, night shade, desert willow, primrose, globe mallow, sand sage, bind weed, scorpion plant, indian rice grass, prickly pear and yucca (Theodore Stans, U.S. Fish and Wildlife Service, personal communication, 1990). The instrumented site is situated within an open space, roughly 6 m x 10 m, that is surrounded mostly by four-wing saltbush (*Atriplex canescens*) with some indigo bush (*Dalea scoparia*) and minor grasses. Figure 4 depicts vegetation type and density at the site.

The depth to ground water is approximately 4 m below land surface. Ground-water recharge occurs primarily by ephemeral stream infiltration from the Rio Salado located about 25 m north of our site and, to lesser extent, by infiltration of precipitation (Stephens et al. 1985, Stephens et al. 1988). For example, within about 20 m of our test plot, there have been two prior studies of recharge by infiltration of precipitation: Phillips et al. (1988) found recharge was about

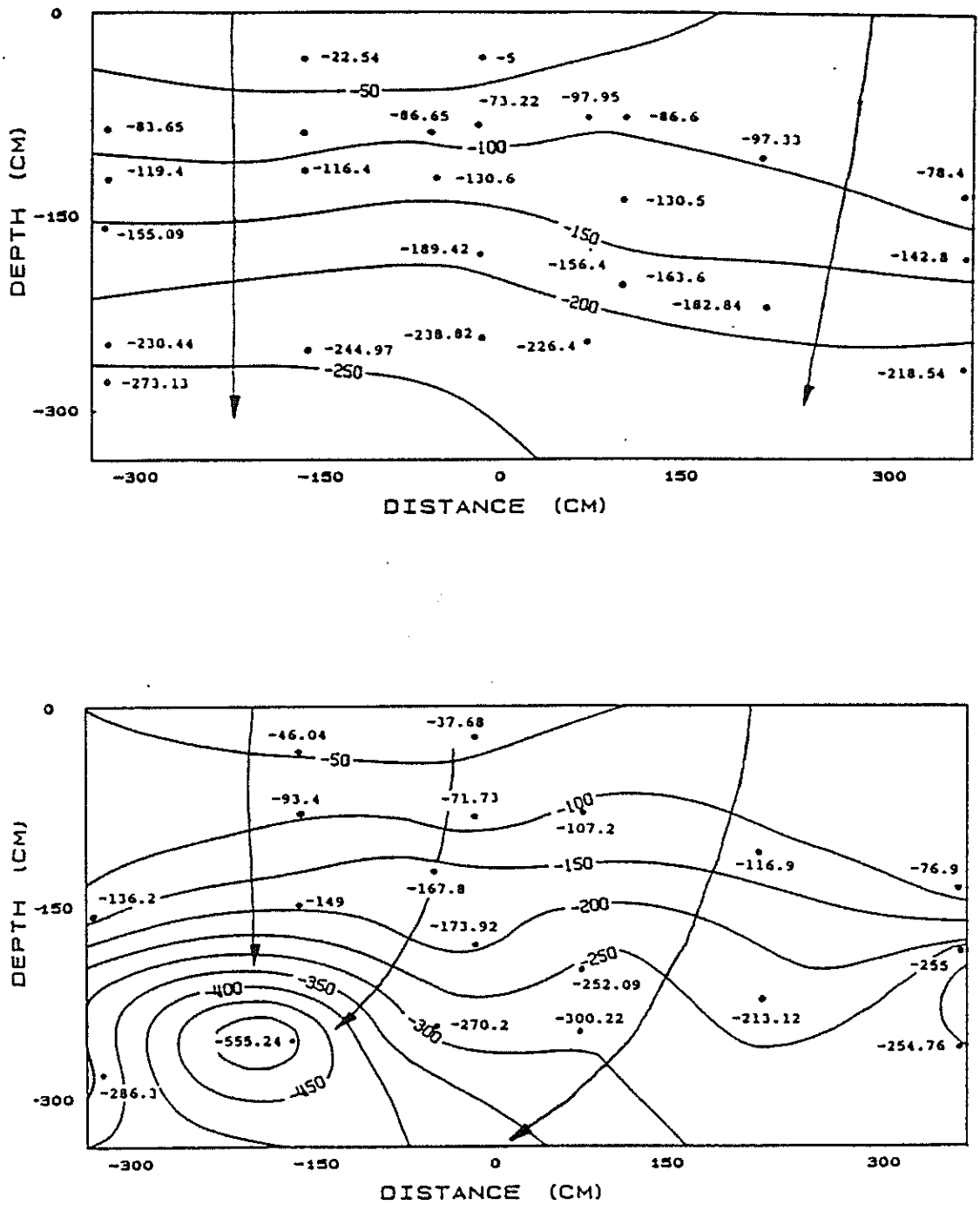

FIGURE 2. Total head in centimeters of water near an indigo sagebush in February 1986 (top) and June 1987 (bottom). Plant trunk is located in the center of the plot (after Kickham 1987).

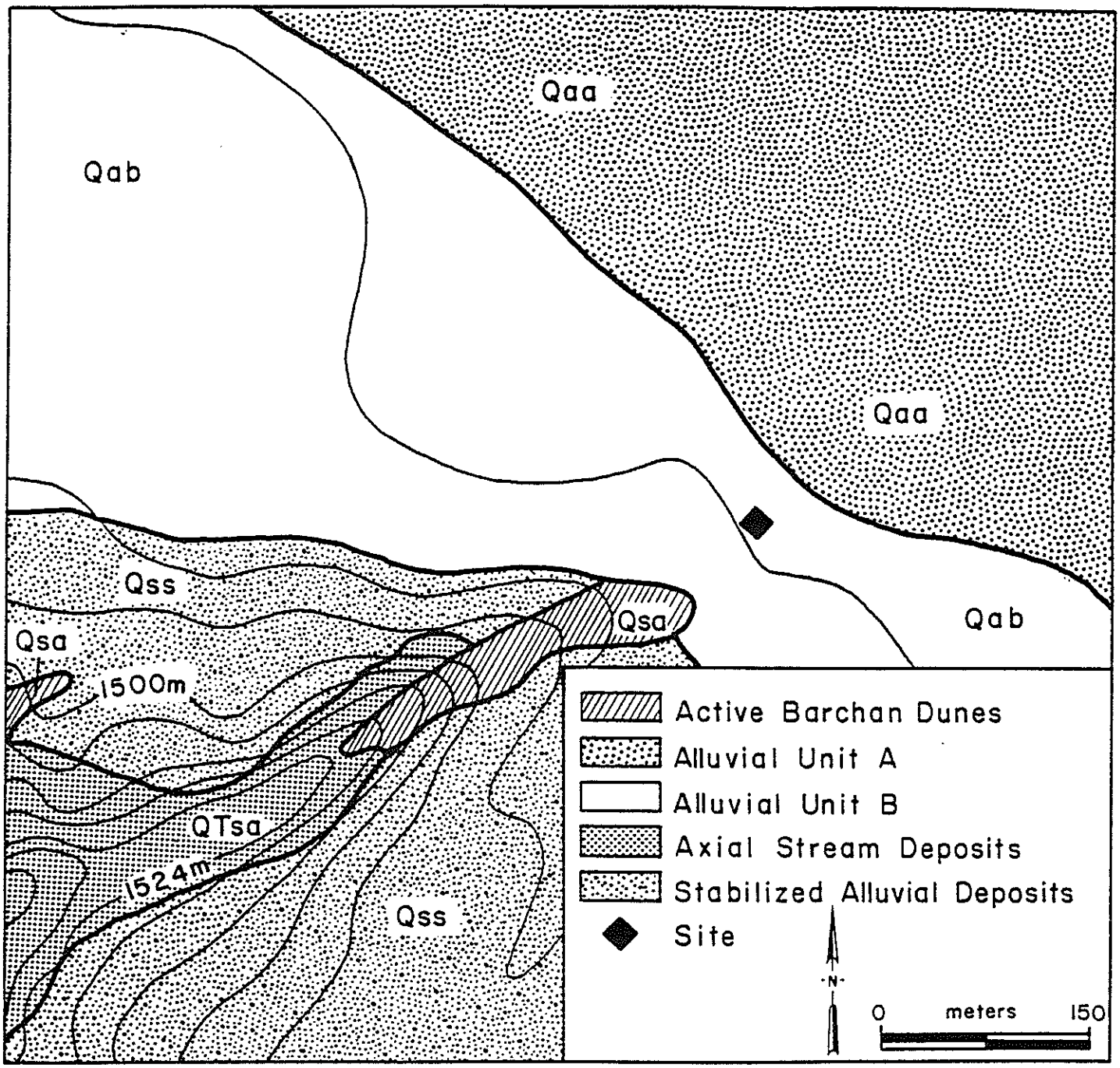

FIGURE 3. Surficial geological map of site.

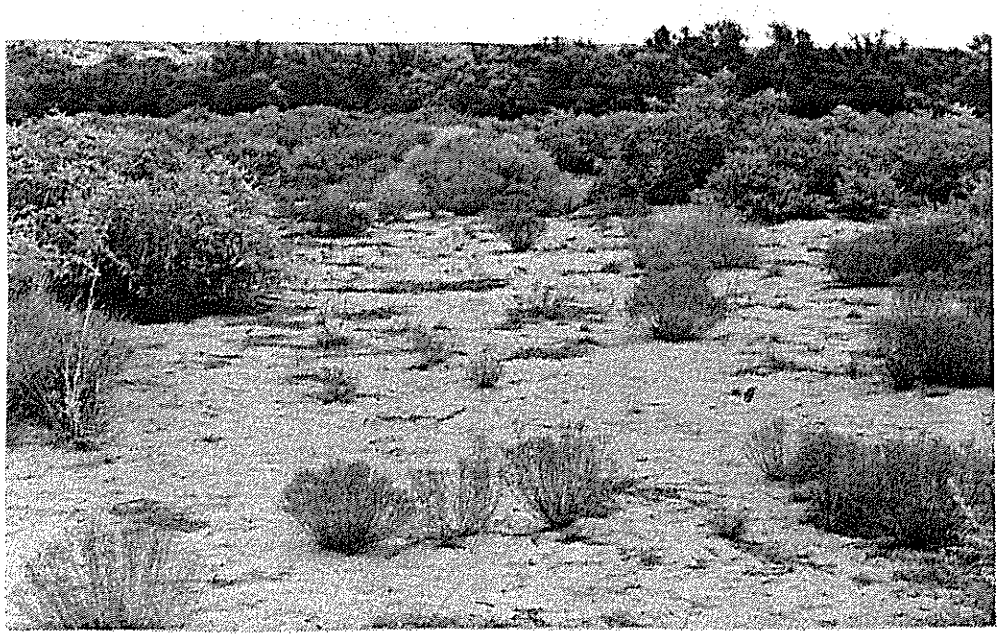

FIGURE 4. Photo of site vegetation.

0.3 to 0.8 cm/yr using chlorine-36 and tritium tracers, and Stephens and Knowlton (1986) calculated recharge to be about 0.6 cm/yr using soil physics instrumentation.

Site Geology and Hydraulic Properties

The site is located on a Holocene flood plain deposit composed of sand with minor amounts of gravel and silt (Figure 3). Samples of soil were obtained at 30 cm intervals from depths of 30 to 480 cm by hand augering and pushing 100 cm^3 core samples into undisturbed soil during installation of neutron probe access tubes (Figure 5). The cuttings were logged for geological characteristics. The core samples were analyzed for in situ moisture content by oven drying at 105°C, saturated hydraulic conductivity was determined with a constant head permeameter after 24 hours, moisture retention characteristics were obtained with a hanging water column and pressure plate, and the particle size distribution was determined on grab samples from one boring (ETN-3) by dry sieving. For detail on the field and laboratory procedures, refer to Stein (1990) and Hicks (1990).

The soil hydraulic properties and their statistical moments are summarized in Table 1. The soil is generally typical of a uniform sand. The geometric mean saturated hydraulic conductivity is approximately 10^{-2} cm/s, median particle diameter is about 0.026 cm, and the parameters of fit (van Genuchten 1980) α, N, and θ_r, to composited θ-ψ pairs from 59 moisture retention curves for drainage are approximated 0.04 cm^{-1}, 2.0, and 0.04 cm^3/cm^3, respectively.

Although the soil appears quite uniform based upon physical properties, there are distinct stratigraphic features that we have identified from geologic analysis of cuttings to 5 m depths and from trenching through the site to nearly 1.2 m at the end of the field program. Geologic cross sections (Figure 6) and saturated hydraulic conductivity values suggest there is a laterally continuous, thin, silty-textured and less permeable (1×10^{-3} cm/s) zone at about the 270 cm depth, and there is a pervasive cobble zone below about 4 m. There is also very fine-scale, horizontal stratification within the more uniform layers, such as in the upper sandy soil shown in the trench (Figure 7).

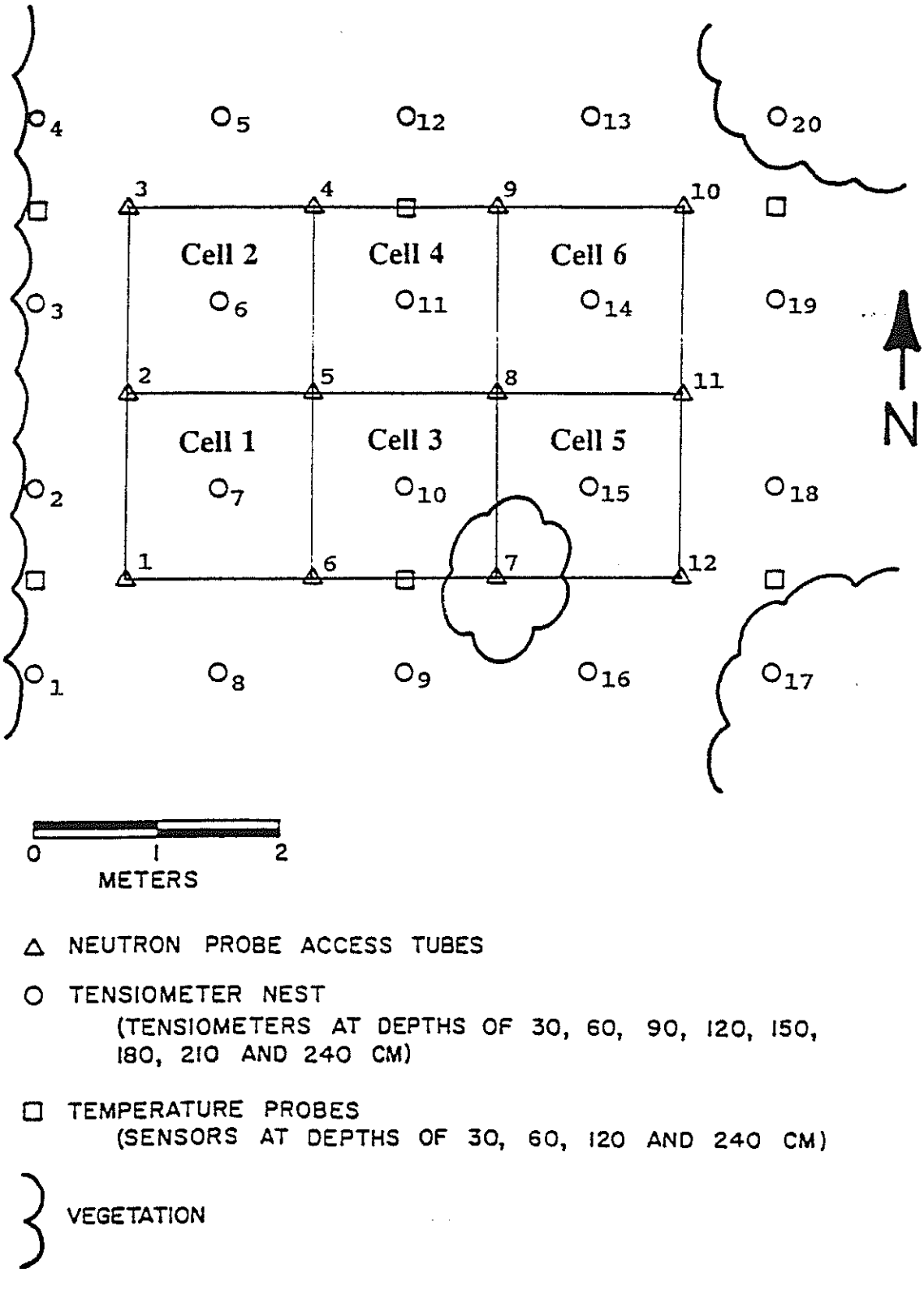

FIGURE 5. Site instrumentation, vegetation, and zones of analysis.

TABLE 1. Summary of Soil Texture and Hydraulic Properties.

PARAMETER	NUMBER OF SAMPLES	MEAN	VARIANCE
10% finer size, d_{10} (mm)	15[a]	0.114	8.64×10^{-4}
50% finer size, d_{50} (mm)	15[a]	0.256	2.34×10^{-3}
uniformity coefficient, C_u	15[a]	2.698	1.70×10^{-1}
saturated hydraulic conductivity, ln K_s (cm/s)	59[b]	-4.656	6.94×10^{-1}
van Genuchten's fitting parameter, α (cm^{-1})	59[b]	4.12×10^{-2}	$1.9 \times 10_{-4}$
van Genuchten's fitting parameter, N (-)	59[b]	2.00	2.1×10^{-1}
van Genuchten's fitting parameter, θ_r (cm^3/cm^3)	59[b]	4.09×10^{-2}	2.57×10^{-4}

[a]Samples from neutron probe access tube ETN-3.
[b]Samples from neutron probe access tubes ETN-1 through ETN-12.

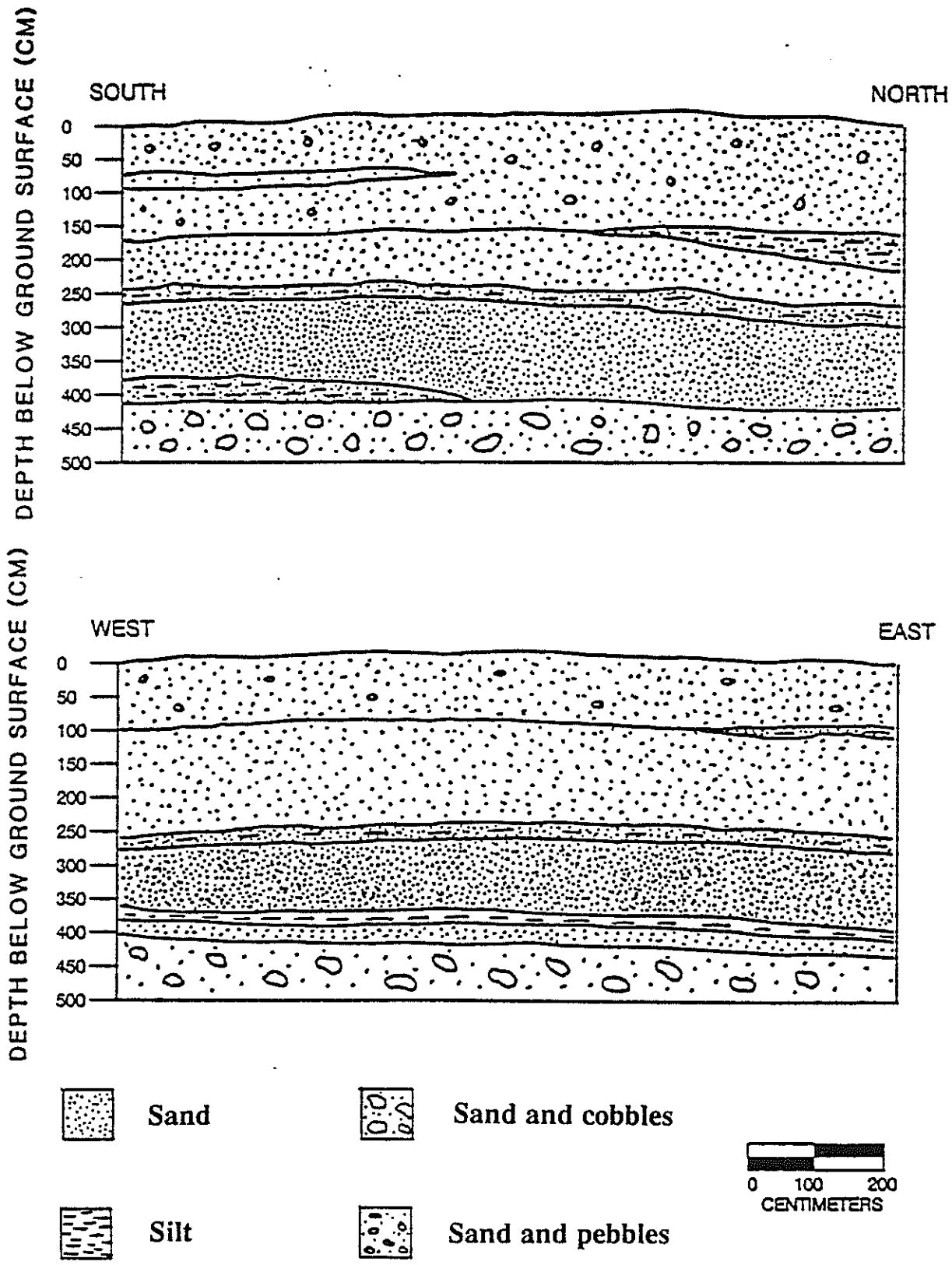

FIGURE 6. Geologic cross sections through center of site.

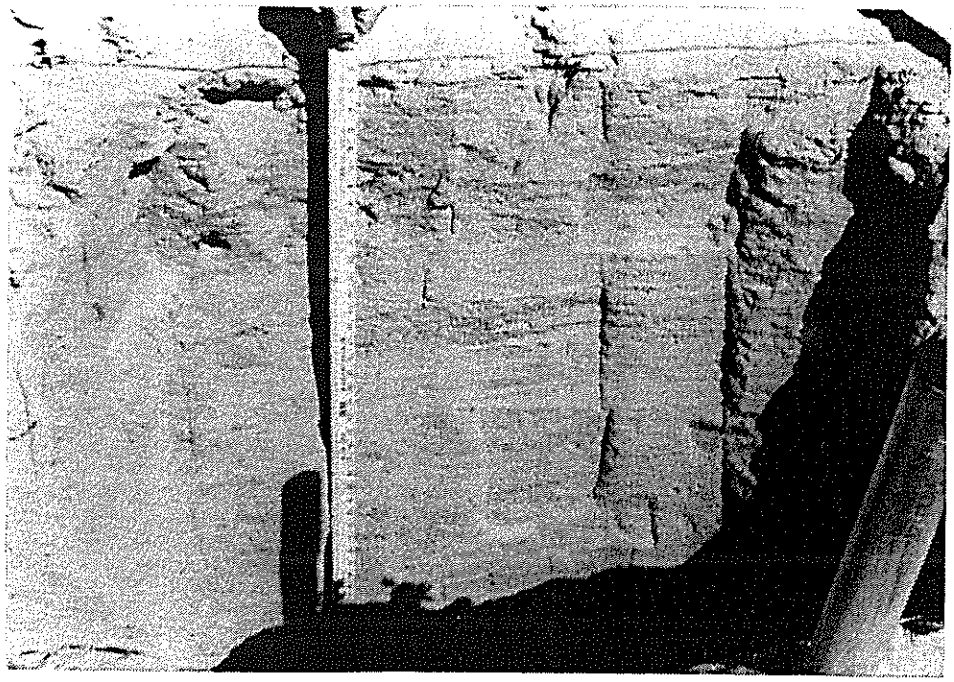

FIGURE 7. Photo of trench showing horizontal bedding features.

Plant Root Systems

The instrumented plot is within a relatively barren area that is surrounded by clusters of native shrubs, mostly consisting of four-wing saltbush (Figure 5). The rooting pattern of the saltbush at the instrumented site was investigated after the in situ soil-water data collection was complete. A trench was excavated from the center of the plot westward to the four-wing saltbush canopy which forms the western edge of the site. Soil and root samples were taken at four different depths from horizontal faces every 40 cm from the canopy. The samples were oven dried overnight, and the roots were separated from the soil by sieving in a number 16 sieve and using forceps to remove any roots which passed through the mesh. The roots were then weighed and compared to the soil's dry weight. The greatest density of roots was expected nearest the canopy. Actually, there was no clear root density pattern (Figure 8). Fine roots were found throughout the 1.2 m deep excavation. However, when neutron probe access tubes were installed, large roots were found to a depth of 4.0 m, near the water table.

The excavation also showed that the roots seek out any disturbance in the soil due to instrumentation installation. Approximately 1.5 years after installation, we noted that the backfill around the aluminum access tubes contained more roots than the surrounding soil. About 1.8 years after installation, two tensiometers were also exposed in the trenching. Both had roots running down their sides, presumably to the ceramic cup. Whether these roots were actually concentrated at the porous cups was not possible to determine, since removing the soil near the cup destroyed the roots and soil clods.

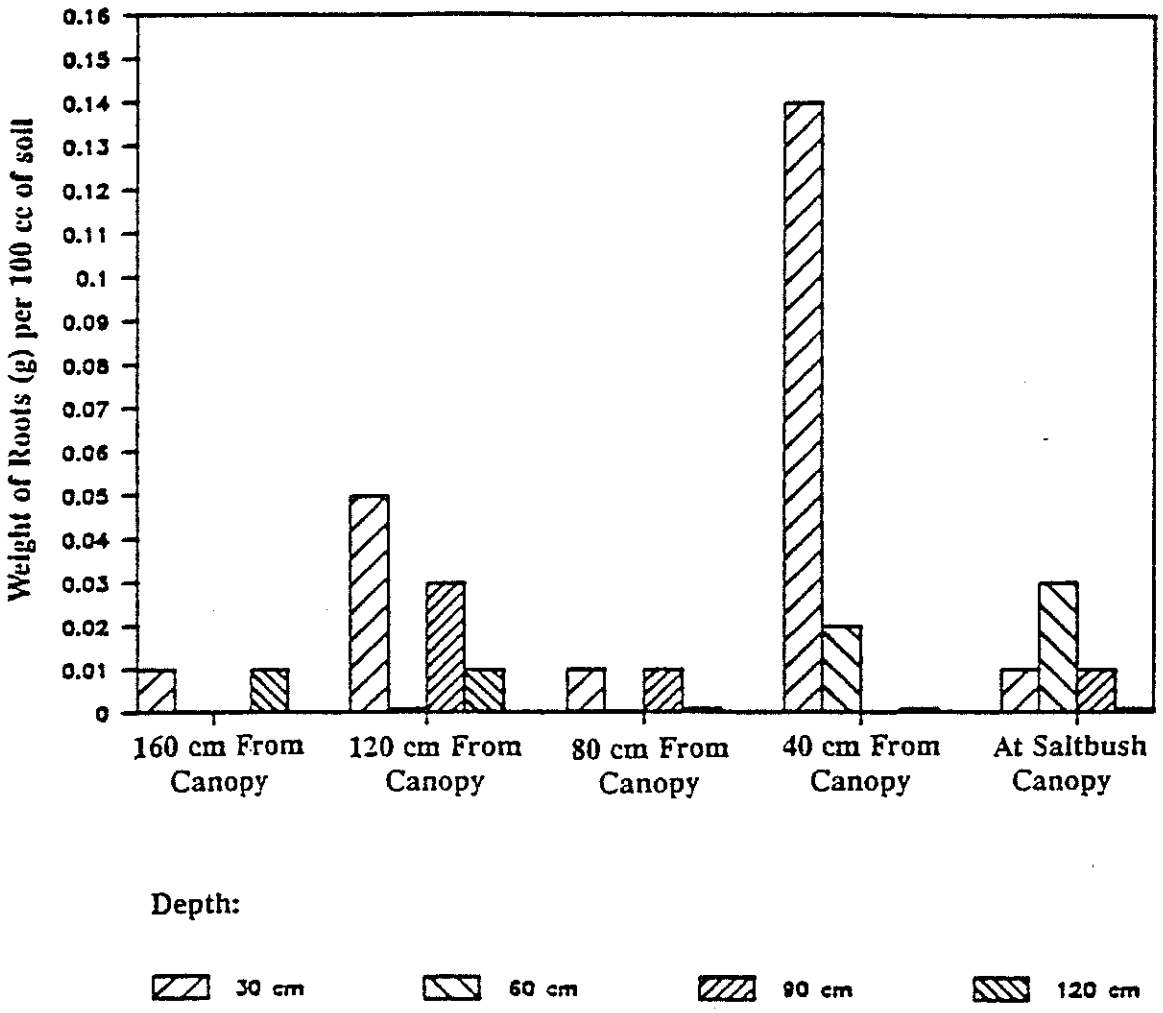

FIGURE 8. Root distribution determined by mechanically separating roots from 100 cm^3 soil core samples.

METHODOLOGY

The field data were used to calculate soil-water flux (volumetric flow rate per unit area) components and an approximate soil-water balance for the field site. The field site was divided into six areas or zones defined by the soil-water instrumentation (Figure 5). Within each zone, the instrumentation also delineated five layers or computational cells. Pressure head and moisture-content data were used to calculate fluxes through each face of the computational cells. Seasonal variations in the direction of soil-moisture movement were examined by using maps of total head in the vertical plane and calculations of horizontal soil-water flux versus time. In addition, vertical fluxes were calculated through the lower-most face of each cell using both measured pressure head gradients and the assumption of a unit hydraulic head gradient. All sets of data were examined for spatial and seasonal patterns in soil-water movement.

Soil-water fluxes across the faces of the computational cells were computed using Darcy's equation,

$$\overline{q} = -K(\theta)\nabla h \qquad (1)$$

where: $\overline{q}$ = soil-water flux (L/T)

$K(\theta)$ = hydraulic conductivity tensor (L/T)

∇h = hydraulic head gradient (L/L)

θ = volumetric water content (L^3/L^3)

Equation 1 is represented in the horizontal directions by:

$$q_x = -K(\theta)[d\psi/dx] \quad or \quad q_y = -K(\theta)[d\psi/dy] \qquad (2)$$

and in the vertical direction by:

$$q_z = -K(\theta)[d\psi/(dz-1)] \qquad (3)$$

where: ψ = pressure head.

The planar faces of the computational cells are located equidistant between the center node and each of the six outer nodes. Consequently, the distance between the center node and each of

the outer nodes is either Δx, Δy, or Δz, as shown in Figure 9. The flux is assumed to be uniform across the face of each cell. Fluxes across the six computational cell faces are calculated from the following equations:

$$\begin{aligned} q_{17} &= K(\theta_{17})[(\psi_1 - \psi_7)/\Delta y] \\ q_{27} &= K(\theta_{27})[(\psi_2 - \psi_7)/\Delta y] \\ q_{37} &= K(\theta_{37})[(\psi_3 - \psi_7)/\Delta x] \\ q_{47} &= K(\theta_{47})[(\psi_4 - \psi_7)/\Delta x] \\ q_{57} &= K(\theta_{57})[(\psi_5 - \psi_7)/\Delta z + 1] \\ q_{67} &= K(\theta_{67})[(\psi_6 - \psi_7)/\Delta z - 1] \end{aligned} \qquad (4)$$

where: ψ_i = pressure head measured at a point indicated by the subscript (Figure 9) and

θ_{ij} = the volumetric water content at the face midway between where ψ_i and ψ_j are measured

These equations are the basis for the three-dimensional analysis of soil-water movement.

Within each of the six subareas (Figure 5), there are five computational cells (Figures 9 and 10). Each of these slices was a computational cell. Each computational cell was 150 cm in both length and width and was 30 cm deep. The corner of each cell face was defined by a moisture content reading made with the neutron probe. The moisture content readings at the four corners of a face were used to calculate an average water content for that face of the computational cell. This value was used to calculate an unsaturated hydraulic conductivity at the average water content for the face using the equation, $K = 5.87 \times 10^{-5} \exp(83.84\ \theta)$. Unsaturated hydraulic conductivity for the alluvial sand was measured in the field by Knowlton (1984) using the instantaneous profile method in the same soil in an area about 10 m just southeast of the current site. Leavitt (1986), who studied the spatial variability of hydraulic conductivity in this area, found no significant difference in mean properties among sites within these sand facies. By using the K-θ relationship, hysteresis problems are avoided.

In calculating the horizontal pressure head gradients, the pressure head at the center of the cell (node 7 in the conceptual model, Figure 10) was found by averaging the pressure head above and below the center of the cell. If one of the tensiometer readings was not available, the other value alone was used to represent the mean pressure head, ψ_7. If both tensiometer data

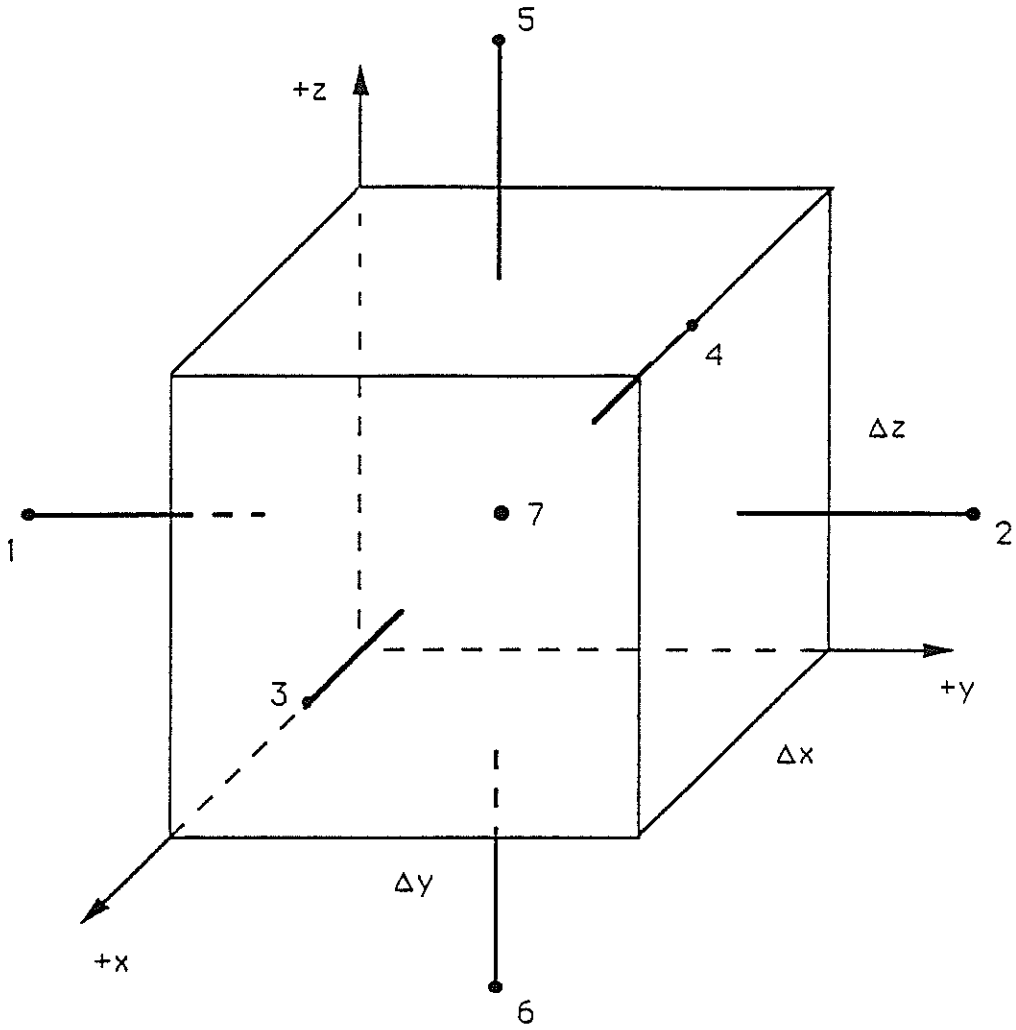

FIGURE 9. Computational cell used to determine soil-water flux.

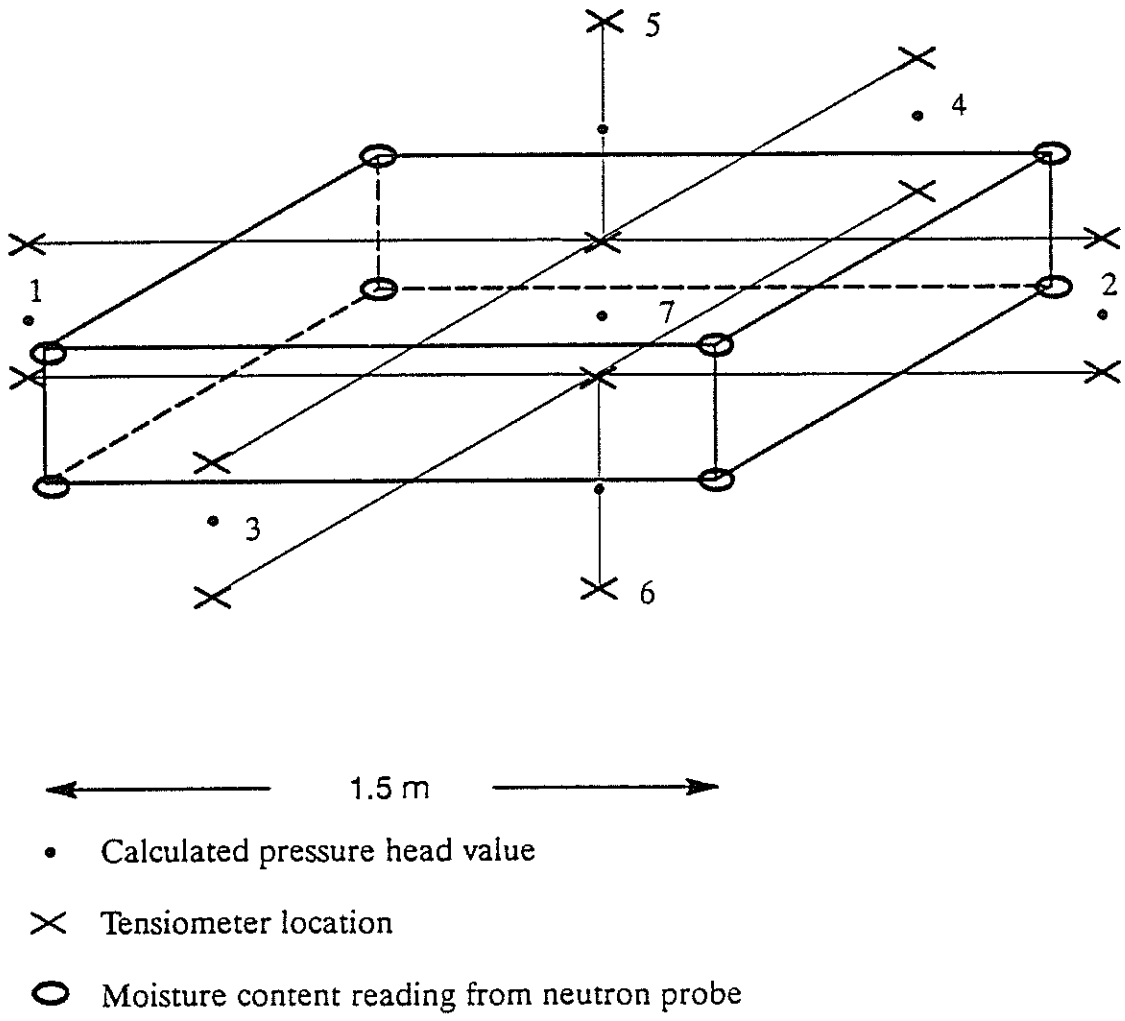

FIGURE 10. Instrumentation used to compute vertical and horizontal fluxes within a computational cell.

were missing, the calculations of pressure at the cell's center could not be made. The pressure head at nodes outside of the cell (e.g., nodes 1, 2, 3, and 4 in Figure 10) was calculated in a similar manner, by averaging two pressure head measurements from tensiometers located above and below this point. The difference in mean pressure head between the center of the cell and nodes (tensiometers) outside of the cell was used to calculate the flux through each of the horizontal faces.

Calculating flux in the vertical direction required a different approach, since there is a different geometry of the tensiometers with respect to the neutron probe measuring points. The pressure head at the top face and the pressure head 30 cm above it were averaged and assigned to the mid-point between these tensiometers (Figure 10). The gradient was then calculated between the average pressure head at that mid-point and the pressure head at the cell's center. In keeping with the sign convention, a positive gradient produces flow into the cell. The flux through the lower face of the cell was calculated in a similar manner except that the gradient was multiplied by -1, since a negative flow rate causes water to leave the cell. We assume that this flux at about 240 cm depth represents recharge, although some water uptake by plant roots may come between 240 cm and the water table. Therefore, the hydrodynamic analysis may over-estimate recharge.

The appendix contains the Fortran code used for the flux calculations. The program stores the water content and pressure-head values in arrays. Using this data, the flux through each face is calculated and the results stored in an array. A running total is also kept of the amount of water which has entered or left each cell for the time period specified. This total can either be expressed as a volume of water per time or a volume of water per unit area.

The methodology presented above describes flow within soil compartments. At a much larger scale, the soil is only one region of the hydrologic cycle. A general approach to a water balance was developed in terms of hydrological processes:

$$P - RO - ET - I - R = \Delta S_1 + \Delta S_2 \qquad (5)$$

where: P = precipitation
RO = surface runoff

ET = actual soil moisture evapotranspiration

I = interception

R = recharge

ΔS_1 = change in soil moisture

ΔS_2 = change in surface water storage

At this site there is little evidence of runoff so we neglect the terms RO and ΔS_2. Because the vegetation is sparse and canopies are thin, we also neglect interception. We compute soil moisture evapotranspiration as the residual, in Equation 5, from measured precipitation and calculated recharge and soil-moisture storage. Soil-moisture evapotranspiration, in this sense, will under-estimate the total evapotranspiration because our analysis neglects water uptake by plants directly from ground water. However, we do account for upward flow of water from the water table by measuring hydraulic gradients and calculating vertical fluxes into the bottom of our soil column.

In as much as the hydrodynamic approach to compute soil-water flux described above is subject to numerous sources of uncertainty, we buried conservative tracers in the soil to confirm the directions of soil-water movement. The tracers included calcium bromide placed 30 cm below land surface, and 2,6-difluorobenzoic acid (2,6-DFBA) placed at 90 cm below land surface (Bowman 1984). To emplace the tracer, a 1.5 cm diameter thin-walled pipe was driven at a 60° angle to the desired depth and a teflon tracer application tube was placed inside. On August 9, 1988, we slowly injected 12.5 ml of 100,000 ppm solutions with a syringe through the teflon tubing, and then we backfilled the hole with native material. This experiment was conducted at four locations: two approximately 50 cm from the center of the saltbush canopy and two about 200 cm from the canopy. On January 24, 1989, the soil-water tracer plots were sampled by vertically driving a thin-walled, 1.5 cm diameter tube at distances of 0, 15, and 60 cm from the location of the applied tracer. The continuous core was sectioned immediately upon return to the laboratory, samples were weighed, mixed with known volumes of distilled deionized water, and prepared for analysis by high performance liquid chromatography (Stein 1990). Each sample represented about 5 cm of soil depth.

INSTRUMENTATION

Pressure Head

The field site was instrumented with 160 tensiometers in a regular grid pattern. Each tensiometer was a ½-inch diameter 1 bar ceramic cup (Soil Moisture Equipment Corp., Santa Barbara, California). The tensiometers were constructed in such a way that a hypodermic needle and transducer (Tensimeter, Soil Measurement Systems, Tucson, Arizona) could measure the pressure in the air space at the top of the tensiometer. From this pressure measurement, we subtracted the height of the water column, measured through a clear acrylic sighting tube, to calculate the actual pressure head in the soil. All measurements were made from the center of the porous cup. Before tensiometers were installed, they were tested in the laboratory for any leaks which would prevent them from maintaining a suction in the field (Hicks 1990).

The tensiometers were placed in a square grid pattern with nests of tensiometers 1.5 m apart (Figure 10). There were twenty nests of tensiometers, with each nest containing eight tensiometers each. The vertical spacing of the tensiometers was 30 cm. The shallowest tensiometer in each nest was 30 cm below datum and the deepest was 240 cm below datum. A level datum at the field site, surveyed from a nearby township marker, was used because the topography at the site varies slightly. The nests of tensiometers were aligned so that the western edge of the grid was parallel to a row of four-wing saltbushes. The northeast and southeast corner of the plot were also located near clumps of four-wing saltbush (Figure 5).

The tensiometers in each nest were offset by 8 cm from the vertical center line of the nest and were staggered in depth around the center line. This was done because tensiometers placed in a vertical nest without any offset may be sensitive to the failure of one of the tensiometers directly above. The center of each tensiometer nest was marked with a stake, and the datum elevation was marked on the stake.

To install the tensiometers, a piece of galvanized conduit, slightly larger in diameter than the tensiometers, was pounded into the soil using a sledgehammer. The soil inside the pipe was removed periodically to facilitate advancement of the boring. After the desired depth was

reached, the tensiometer was placed in the hole. As the tensiometer was backfilled, it was twisted slightly and moved from side to side to make sure the ceramic cup was in contact with the soil.

An antifreeze solution containing ethylene glycol was used in the tensiometers to prevent them from freezing and cracking (Knowlton 1984, McKim et al. 1976, Wendt et al. 1978). The exposed portions of the tensiometers were shaded by covers made from 6.25 cm diameter PVC pipe 30 cm long (Hicks 1990). These covers prevented the sunlight from bleaching the markings on the tensiometers and protected the PVC and rubber stoppers from ultraviolet light which makes them brittle.

The tensiometers were maintained so that their fluid level and air gap were measurable in the sight glass. During the course of this investigation, Hicks (1990) observed that the pressure inside of the tensiometers could be affected by several tens of centimeters by daily changes in temperature (Figure 11). The conductance of the tensiometer cup apparently was not sufficiently large to allow rapid equilibration between pressure in the tensiometer and soil-water potential. The best time to read tensiometers was when the temperature had remained relatively constant, so that the pressure inside the tensiometer was close to equilibrium with the soil-water potential. We monitored the tensiometers in the early morning before the sun struck them.

Moisture Content

At the research site, the neutron scattering technique was used to indirectly measure water content in the soil. The neutron probe (503DR, Campbell Pacific Nuclear, Martinez, California) had a 50 millicurie americium-242/beryllium source of fast neutrons. The probe was calibrated for the Sevilleta soil as described by Stephens et al. (1985). Thin-walled aluminum access tubes (5 cm in diameter) were installed at locations in the grid shown in Figures 10 and 12. The neutron access tubes were installed by hand augering holes with a 6 cm diameter auger bit. The bottom of each access tube was capped with a rubber stopper and sealed with silicon adhesive to prevent moisture from seeping into the tube. After inserting the access tubing, the annular space was backfilled with dry native sand to ensure proper contact between the soil and access tubing.

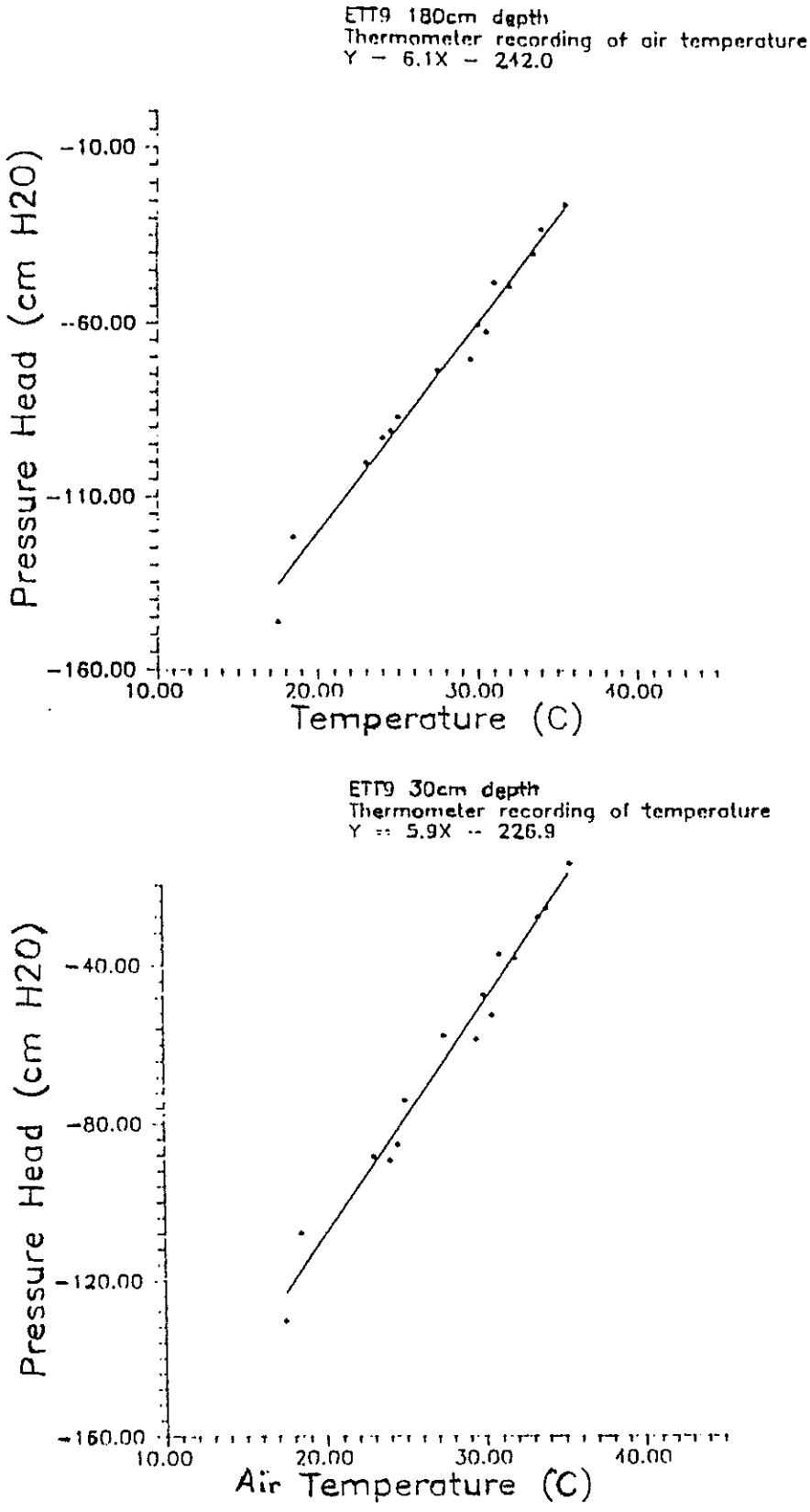

FIGURE 11. Temperature effect on tensiometers.

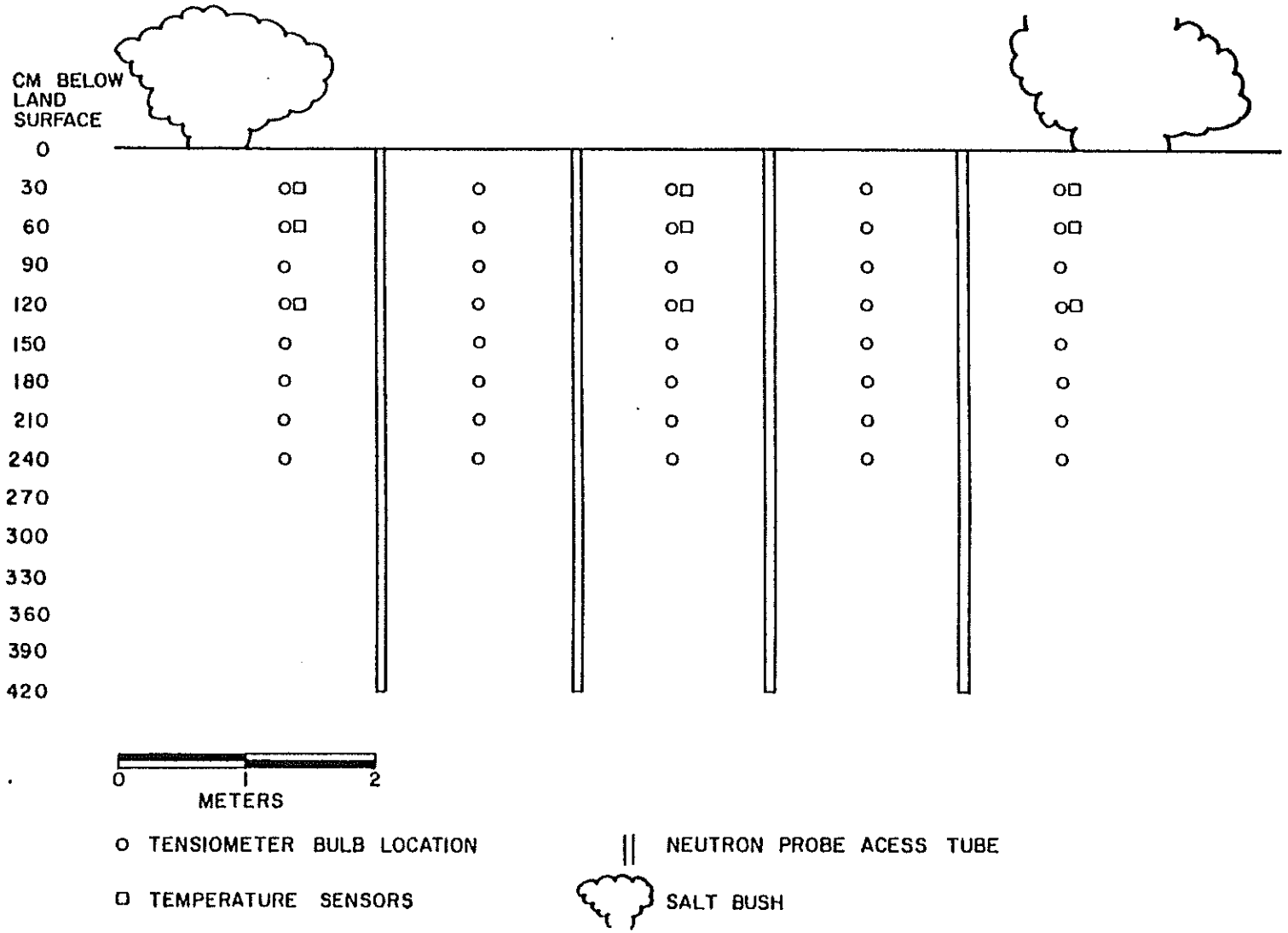

Figure 12. Vertical cross section of instrumentation.

The neutron probe access tubes were installed to a maximum depth of 480 cm, except wherever cobbles prevented us from hand-augering further. Neutron probe readings were taken at 30 cm intervals beginning at a depth of 30 cm below the field datum, the highest point within the research site, as described previously for the tensiometers. Readings were taken at a count time of 16 seconds. At this counting time, the standard deviation of the measurement (caused by variations in neutron production) ranged from about 0.1% to 1.3% of the measured value.

Climatological Data

An automated weather station was located a few meters to the south of the field site. A data logger (21X Micrologger, Campbell Scientific, Logan, Utah) was used to record weather data. Data was stored in internal memory until it was manually downloaded to a cassette tape recorder. The tape was then taken to the laboratory where a cassette interface (C20, Campbell Scientific, Logan, Utah) transferred data to an ASCII file on a personal computer. The field measurements included: precipitation, air temperature, relative humidity, wind speed, wind direction, and solar radiation (Hicks 1990, Stein 1990). In the early summer of 1988, soil temperature measurements were also made by thermistors set at 6 locations in the soil profile at depths of 30, 60, 120, and 240 cm.

Another weather station was located about 0.5 km west of the plot. Meteorological instrumentation at this site included a tipping bucket rain gage, maximum-minimum thermometer, Class A evaporation pan, and totalizing anemometer (Stein 1990).

RESULTS AND DISCUSSION

In this section we present first the precipitation data, and then our results of the flow field that were interpreted from tensiometer data. Using the hydraulic head data to compute fluxes for the computational cells, we then describe the results of the moisture-content monitoring. Finally, we present a composite water balance for the site.

Precipitation

Precipitation was measured from December 1987 to August 1989. During 1988, precipitation totalled 17.7 cm, which is slightly below the mean precipitation recorded at this site since late 1982 (Table 2). During the course of most of the field work (July 1988 to July 1989), the largest portion of precipitation occurred in mid to late summer, and the winter precipitation was less than normal compared to the prior years of record. Monthly precipitation is shown in Figure 13 (Hicks 1990).

Soil-Water Flux Analysis

Pressure head data from selected tensiometers located along an east-west transect is shown in Figure 14. The transect includes tensiometer nests 3, 6, 11, 14, and 19 as shown in Figure 5. The pressure head data plotted in Figure 14 were not corrected for temperature effects. This correction and all raw data are presented in detail by Hicks (1990). In general, the tensiometric data showed the wettest period was in the late summer and early fall of 1988, in response to summer precipitation (Figure 13). Late winter precipitation in January and March 1989 also increased soil moisture. During most of the spring and summer of 1989, the soil drained steadily at all depths, but drying is most noticeable at the 30 cm depth.

Several methods were used to analyze the pressure head data from the tensiometers. The most convenient method to evaluate the direction of moisture flow is to construct a flow field based on hydraulic head values (Figure 15 a,b,c,d). We infer here that the direction of flux is parallel to the hydraulic gradient. Most cross sections show a predominant downward movement of water with little lateral flow, even in the summer. The cross section of October 15 (Figure 15b)

TABLE 2. Composite Precipitation Data at the Sevilleta Research Site, 1982 to 1989 (Stephens et al. 1985, Kickham 1987).

	1982	1983	1984	1985	1986	1987	1988	1989	MEAN
JAN		44.5	7.8	3.9	5.8		7.5	16.5	14.3
FEB		31.2	0.0	3.5	5.8		15.0	2.5	27.3
MAR		7.9	0.4	18.3	2.3		0.5	17.0	7.7
APR		3.3	0.4	22.0	2.0		21.0	1.5	8.4
MAY		7.0	0.0	11.1	22.1		9.0	0.0	8.2
JUN		5.7	5.8	11.6	28.2		15.5	0.0	11.3
JUL		1.2	2.8	15.0	17.8		19.9	36.0	15.4
AUG		17.9	15.3	21.8	20.1		35.0	1.0	18.5
SEP		60.9	22.3	25.0			47.0		38.8
OCT		12.4	52.5	63.2			1.0		32.3
NOV	18.3	9.5	17.2	2.4			2.5		10.0
DEC	32.3	5.1	31.5			22.0	3.0		18.8
TOTAL		206.6	156.0				176.9		211.0

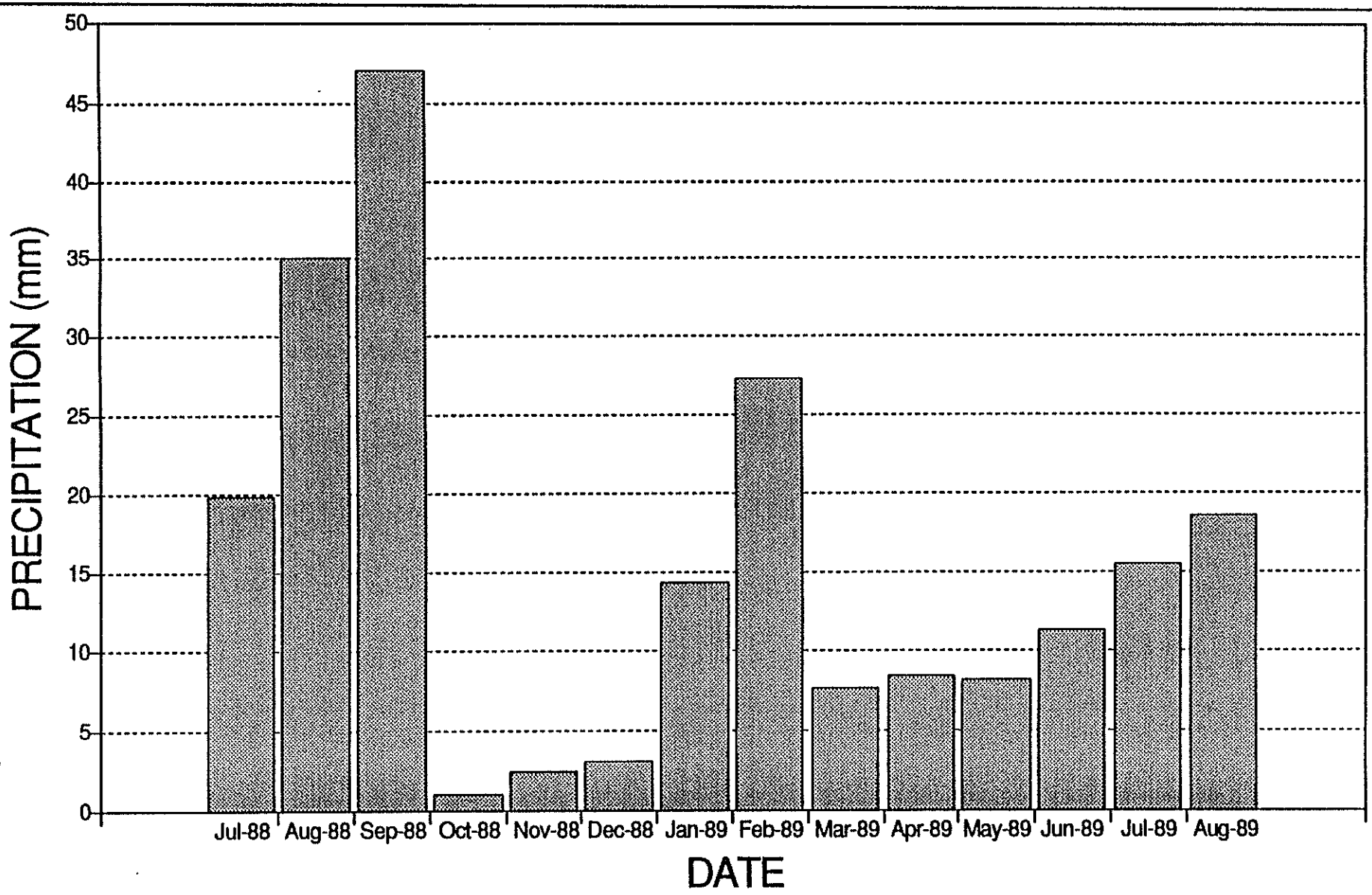

FIGURE 13
PRECIPITATION DATA
JULY 1988 THROUGH AUGUST 1989

DATE	PROJECT NO	DESIGNED BY	DRAWN BY	CHECKED BY

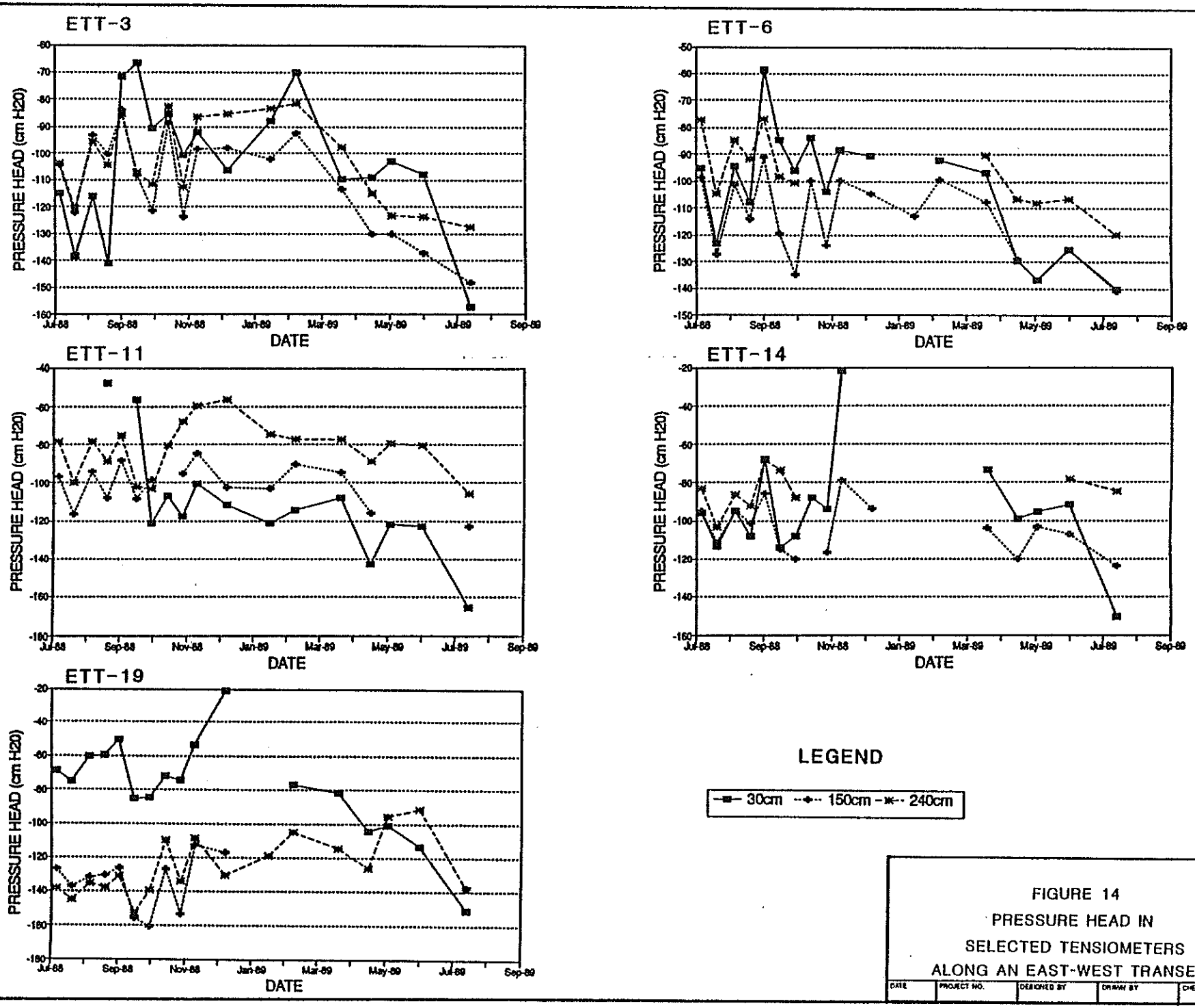

FIGURE 14
PRESSURE HEAD IN
SELECTED TENSIOMETERS
ALONG AN EAST-WEST TRANSECT

DATE	PROJECT NO.	DESIGNED BY	DRAWN BY	CHECKED BY

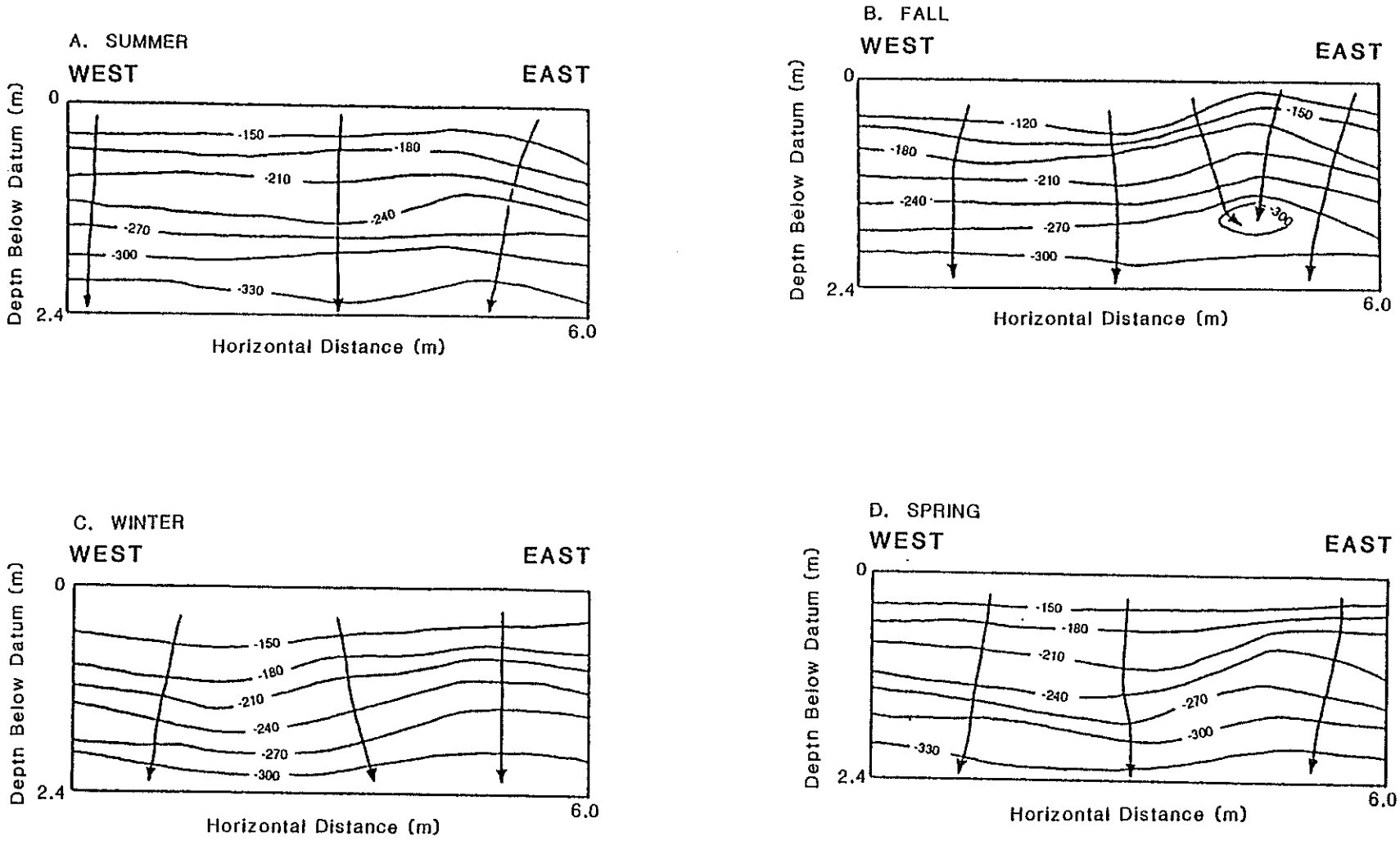

Figure 15. Hydraulic head and gradient direction along north edge of plot (tensiometer nests 4, 5, 12, 13, and 20) (Figure 5): (a) July 20, 1988, (b) October 15, 1988, (c) December 9, 1988, (d) April 21, 1989.

is the only one to show converging flow, and this inexplicably occurred in the east-central part of the plot where surface vegetation was sparse. These figures illustrate qualitatively that the horizontal flow components are much smaller than the vertical components. These components are quantified in the following sections.

Horizontal Flux. We used the computer code described earlier (appendix) to calculate both direction and magnitude of the soil-moisture flux based on pressure head gradient and hydraulic conductivity at the field water content (Equations 2 and 3). The pressure head data were analyzed to identify seasonal variations in the magnitude and direction of the horizontal flux components for several different cells, and data for cell 1 (Figure 10) are shown in Figures 16 through 18. The horizontal component of soil-water flux on the vegetated west side of the plot was as much as about 10^{-3} cm/d, but typically the horizontal flux averaged much less, about 10^{-5} cm/d. Results in Figure 16 indicate that the maximum horizontal flux occurred in summer, and at this time there was a westward flow component toward the saltbush cluster on the west side of the plot, as we expected. However, during the fall and winter of 1988 the soil-water flux across the west face was to the east, opposite to the horizontal component of flux in the mid-summers of 1988 and 1989. One explanation for the apparent variability in direction of horizontal soil-water movement might be interception of rainfall by the canopy of the four-wing saltbush, inasmuch as the root density appeared to be relatively uniform within the plot. We did not identify any other significant seasonal variability in horizontal soil-water flux near the densely vegetated west side of the plot.

Observed fluxes through the north face of zone 1 are shown in Figure 17. Compared to flux across the west face, in the north face there is less of a seasonal pattern noted in the earlier months, but there seems to be a northerly trend during June and July near the end of the study. The fluxes at each depth remained fairly constant in their direction through the summer to the winter of the first year. Intuitively, we expected fluxes due to water uptake by plants to diminish during the winter. However, as we will discuss later, the magnitude of many of the fluxes is so small relative to the uncertainty in the data that some of the values may be unreliable.

Figure 18 shows the fluxes calculated through the east face of zone 1. Compared to the west face of this zone (Figure 16), this face is 150 cm farther away from the line of saltbushes located along the western edge of the experimental plot. The flow field here is more difficult to

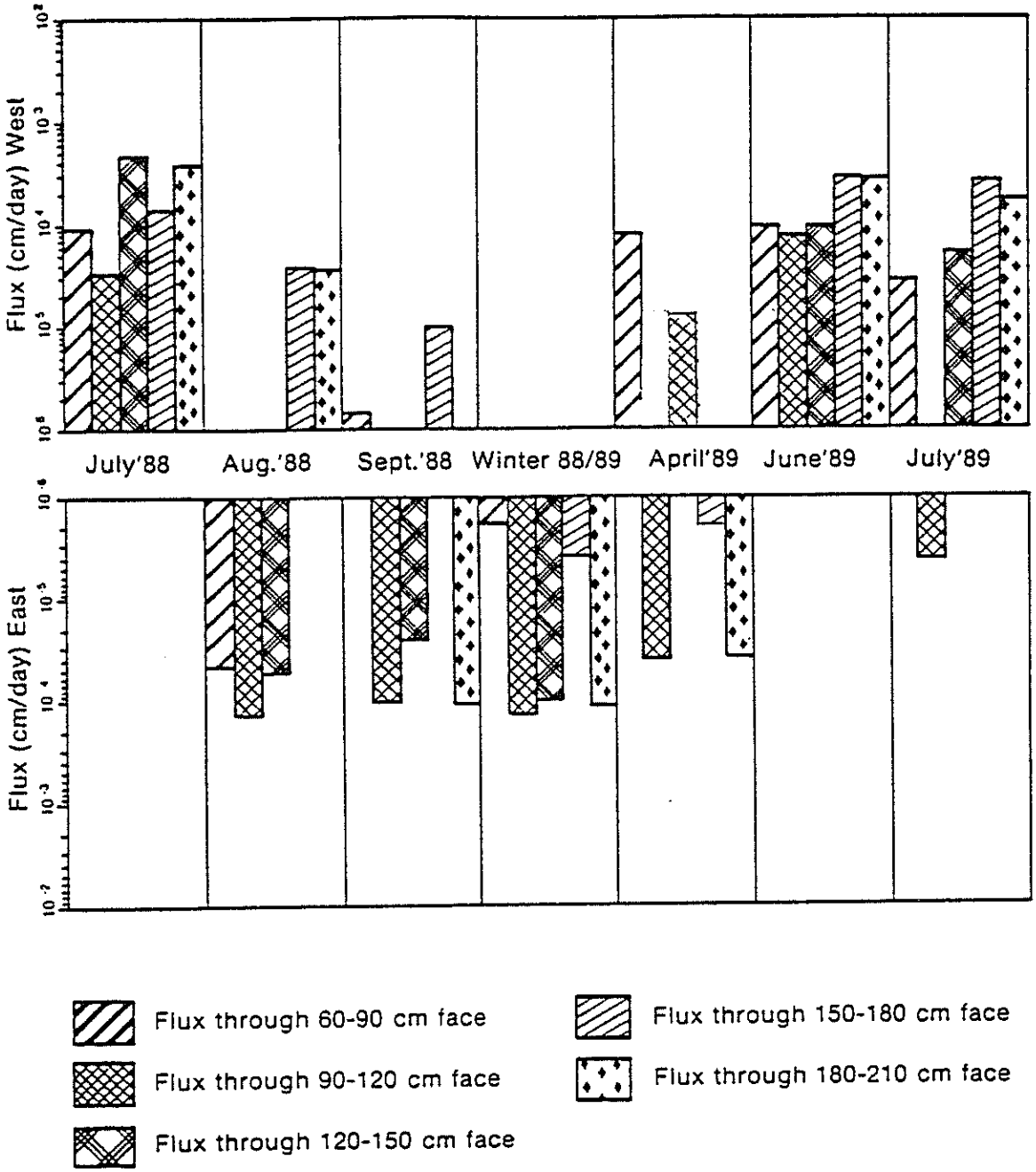

FIGURE 16. Horizontal flux through the west side of cell 1.

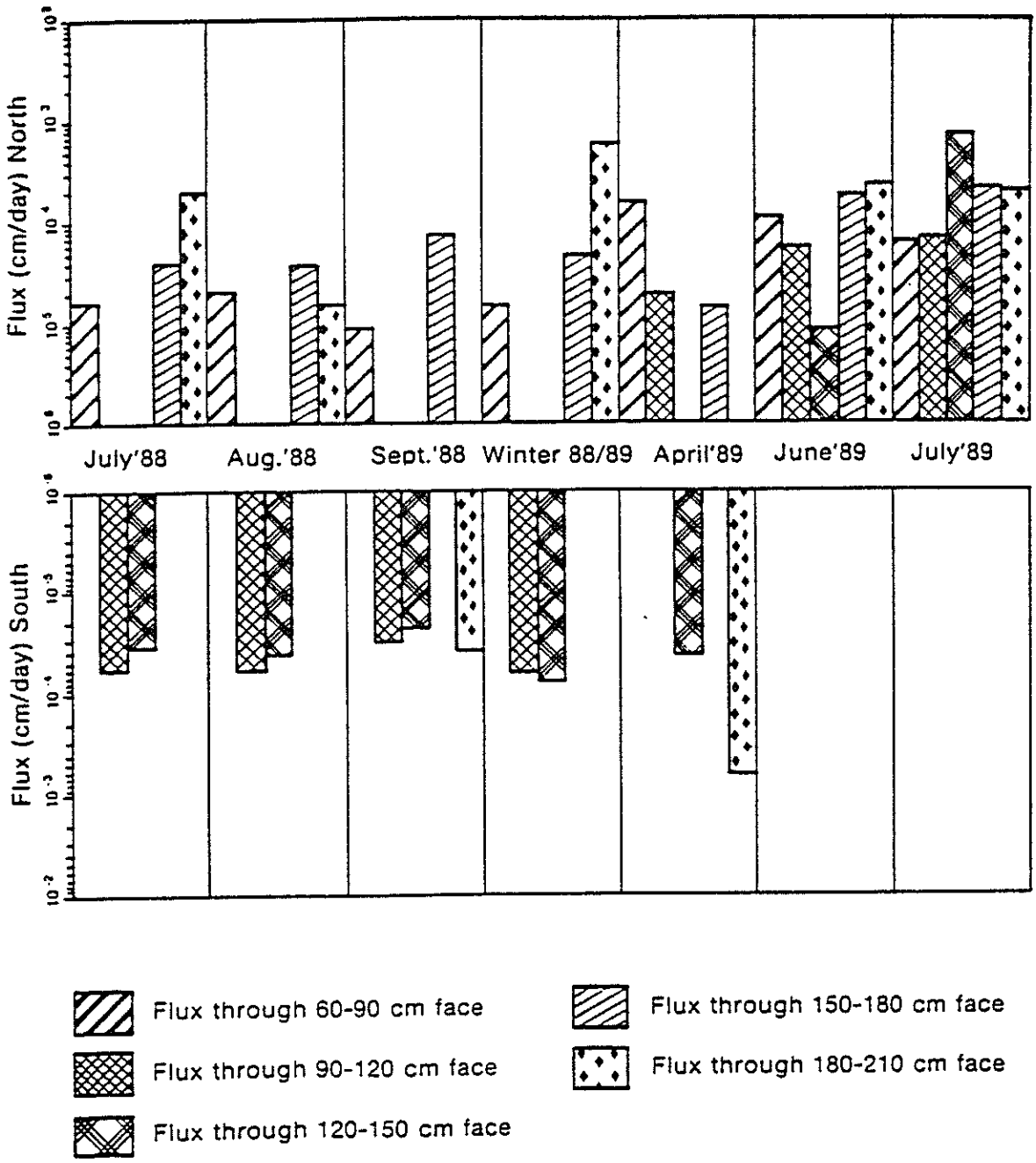

FIGURE 17. Horizontal flux through the north side of cell 1.

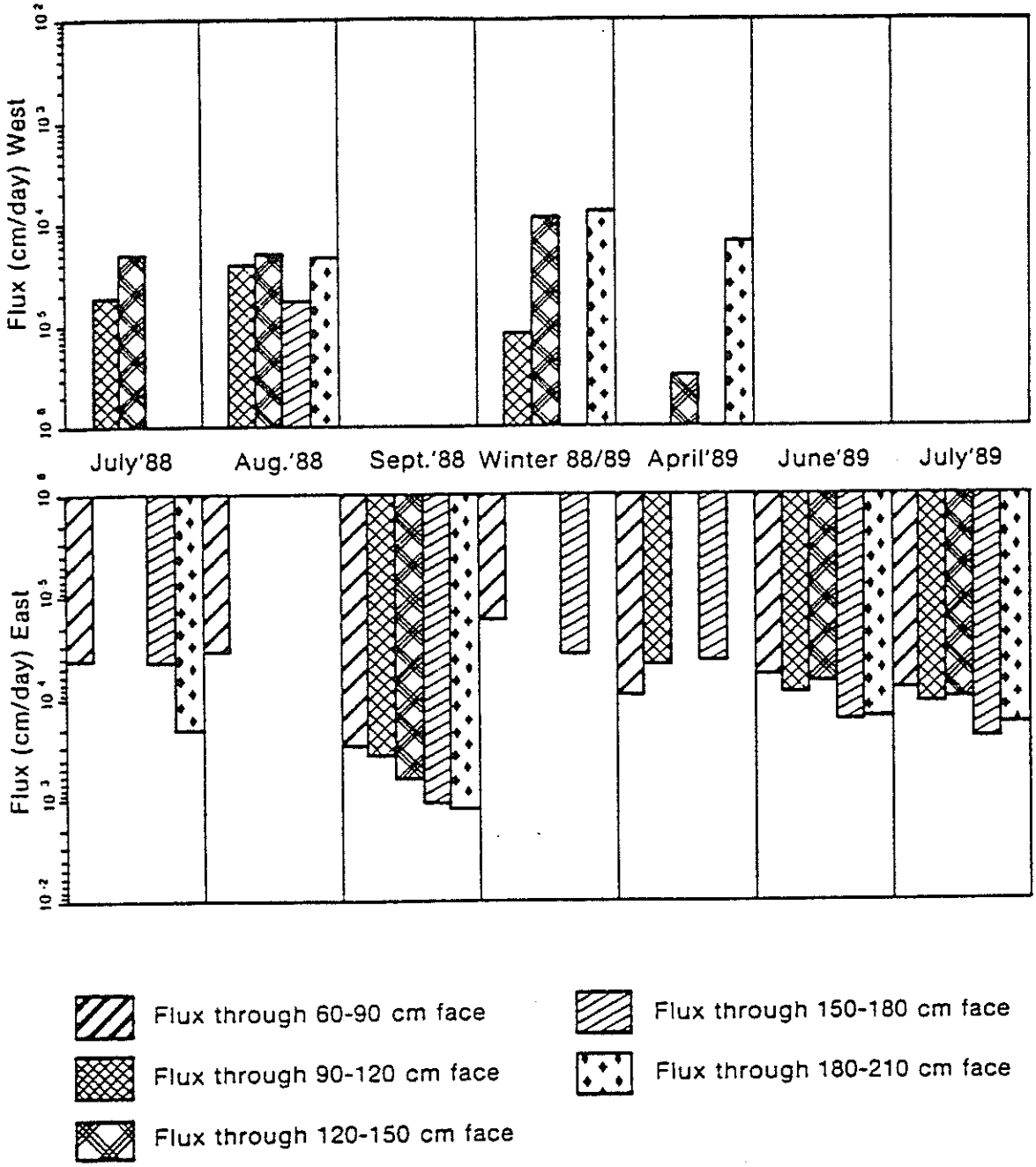

FIGURE 18. Horizontal flux through the east side of cell 1.

interpret because this face is about the same distance from an indigo sagebush as it is from the saltbush (Figure 5), and there might be two competing root systems affecting horizontal water movement across this face. In July and August, the horizontal flux was relatively small. However, in September 1988, large horizontal fluxes occurred at all depths. As shown in Table 2, about 8 cm of precipitation fell in August and September 1988, and this may have caused a sufficient increase in moisture throughout the profile to increase fluxes at all depths. The winter and April fluxes are more variable, as is the precipitation, but in June and July horizontal soil-water movement was all eastward toward the indigo bush. The magnitude of the horizontal flux diminished in September, possibly due to the increase in soil moisture available to plants following the summer rains.

Overall, the lateral fluxes calculated are not very definitive. Error in their calculation from field measurements makes for noisy data, which is difficult to interpret. The fluxes from the face nearest the saltbushes do seem to reflect the influence of the bushes, in that there are some seasonal changes in the fluxes. However, it is difficult to explain the way the flux directions appear to reverse. Toward the center of the plot and away from the large bushes, it is more difficult to find any seasonal patterns of horizontal soil-water movement.

Vertical Flux. For each of the six zones, the flux through the bottom face (below 210 cm depth) of each computational cell was calculated for seven different time periods. The results are shown in Table 3. We infer here that soil-water flux at the 2.1 m depth eventually becomes recharge to the aquifer which is about 4 m below land surface. However, some depletion of moisture probably occurs below this depth based on our observations of roots. Consequently, recharge calculated from vertical soil-water flux at the 2.1 m depth may be an over-estimate. On the other hand, the accumulation of roots which we observed in the vicinity of the tensiometers and neutron probe access tubes could give rise to local hydraulic conductivities which underestimate average conditions, and this would cause the calculated recharge to be less than values shown here. Other sources of error are discussed later.

TABLE 3. Estimated recharge rates based on measured pressure head and water content, 210 cm depth. (Positive values indicate downward flux.)

TIME	FLUX (cm/day)					
	ZONE 1	ZONE 2	ZONE 3	ZONE 4	ZONE 5	ZONE 6
July 1 - July 31	8.45×10^{-4}	6.34×10^{-4}	6.56×10^{-4}	4.41×10^{-4}	2.59×10^{-4}	-1.46×10^{-5}
July 31 - August 25	7.61×10^{-4}	5.13×10^{-4}	9.41×10^{-4}	2.63×10^{-4}	5.73×10^{-4}	-1.22×10^{-4}
51 days - October 15	5.54×10^{-4}	3.50×10^{-4}	1.47×10^{-3}	4.75×10^{-4}	2.45×10^{-4}	6.77×10^{-5}
October 15 - February 15	4.82×10^{-4}	1.09×10^{-3}	3.39×10^{-4}	6.73×10^{-5}	7.73×10^{-4}	3.54×10^{-3}
February 15 - March 16	3.32×10^{-3}	4.33×10^{-4}	2.69×10^{-6}	2.34×10^{-4}	8.41×10^{-4}	6.96×10^{-4}
March 16 - June 30	9.24×10^{-4}	3.76×10^{-4}	9.33×10^{-5}	2.62×10^{-3}	8.88×10^{-4}	2.60×10^{-4}
July 1 - July 31	1.97×10^{-3}	3.90×10^{-4}	3.05×10^{-4}	2.62×10^{-4}	8.37×10^{-4}	-1.75×10^{-4}
Recharge (cm/yr)	1.02	0.234	0.166	0.164	0.249	0.540
Percent of Precipitation*	5.67	1.30	0.92	0.91	1.38	3.00

*Based on annual precipitation of 18 cm

Over the six cells, recharge ranged from 0.9% to 5.7% of annual precipitation. The time-weighted average vertical flux was about 0.4 cm/yr; this comprises about 2.2% of annual precipitation based on a mean annual precipitation of about 18 cm/yr. As described above, the lateral fluxes were about one hundred-fold smaller, usually about 3.6×10^{-3} cm/yr (1.0×10^{-5} cm/day). Recharge calculated from this approach is comparable to other methods, as will be described later.

We also computed recharge based upon the assumption of a unit hydraulic gradient, that is, by neglecting horizontal flow components. The only driving force of the soil is assumed to be gravity. This method is often used as a quick estimate when pressure head data are not available. The water content and the corresponding unsaturated hydraulic conductivity are the only model inputs (Equation 3). The results of the unit gradient method of calculating deep fluxes are found in Table 4. There is less spatial variability in the vertical fluxes calculated with the unit gradient assumption compared to fluxes calculated using actual pressure head measurements shown in Table 3. Nevertheless, estimated recharge rates based on the pressure head data and the unit gradient assumption are in fairly close agreement. The mean recharge by the unit gradient analysis is about 0.29 cm/yr, compared with 0.40 cm/yr by including measured pressure head gradient. Over the period of record, the mean hydraulic gradient was about 1.4, based upon the ratio of mean flux from pressure head measurements and flux from the unit gradient assumption. It is important to recognize, however, that the gradient, and therefore soil-water flux, are actually not uniform over the entire plot.

When the calculated hydraulic gradient is included in the analysis, the greatest amount of recharge, 1.02 cm/yr, is calculated in zone 1, which was closest to the saltbush, and the least amount of recharge was near the relatively unvegetated center of the plot at zones 3 and 4. This result suggests that the saltbush intercepts a significant amount of snowfall which leads to greater infiltration near the bush. It is likely that evaporation across the soil surface near the plant canopy could be smaller than near the exposed center of the plot because of the shelter from the wind and sun. Furthermore, near the canopy there is a thin mulch of fallen plant material to slow evaporation. However, cell two, which is also located adjacent to the saltbushes, had a relatively low predicted recharge rate of only 0.23 cm/yr. It is also possible that a tensiometer failure led to errors in the gradient calculations.

TABLE 4. Estimated recharge rates based on assumed unit gradient and water content measurements, 20 cm depth.

TIME	FLUX (cm/day)					
	ZONE 1	ZONE 2	ZONE 3	ZONE 4	ZONE 5	ZONE 6
182 - 212	1.08×10^{-3}	1.04×10^{-3}	9.94×10^{-4}	8.95×10^{-4}	1.01×10^{-4}	8.76×10^{-4}
212 - 257	9.33×10^{-4}	8.58×10^{-4}	9.14×10^{-4}	6.81×10^{-4}	8.95×10^{-4}	7.26×10^{-4}
237 - 288	8.95×10^{-4}	8.40×10^{-4}	9.53×10^{-4}	6.96×10^{-4}	8.95×10^{-4}	7.26×10^{-4}
288 - 439	8.58×10^{-4}	8.23×10^{-4}	8.58×10^{-4}	6.96×10^{-4}	7.73×10^{-4}	6.53×10^{-4}
439 - 500	7.73×10^{-4}	7.41×10^{-4}	8.06×10^{-4}	6.67×10^{-4}	8.06×10^{-4}	6.96×10^{-4}
500 - 546	7.26×10^{-4}	6.81×10^{-4}	7.57×10^{-4}	6.53×10^{-4}	7.26×10^{-4}	6.67×10^{-4}
546 - 577	7.41×10^{-4}	7.41×10^{-4}	7.89×10^{-4}	6.67×10^{-4}	7.26×10^{-4}	6.53×10^{-4}
Recharge (cm/yr)	0.309	0.295	0.314	0.255	0.296	0.253
Percent of Precipitation*	1.72	1.64	1.74	1.42	1.64	1.41

*Based on annual precipitation of 18 cm

In contrast to the pressure head-based analysis, the unit gradient approach indicates that the highest recharge rate occurs in the center of the plot were the soil is slightly more moist. By the unit gradient analysis, the lowest recharge rate occurs in cell six which has a clump of saltbush near its corner. Over the six cells, the spatial differences in recharge are relatively small by either analysis. During the period of record, these two different methods predict, on average over the six cells, that about 2.2% to 1.6% of precipitation (18 cm) becomes recharge. These methods compare favorably with one another, but both use the same unsaturated hydraulic conductivity function that is a crucial parameter in the flux analysis.

The computed fluxes are based on field data and have the usual errors associated with measuring and installing field instruments as well as errors due to other sources. For example, all of the flux calculations are based on hydraulic conductivity and pressure head measurements. Unsaturated hydraulic conductivity is a very difficult value to measure in the field at low water contents. Some researchers consider one order of magnitude the best one can estimate unsaturated hydraulic conductivity (Gee and Hillel 1988). In our study we assumed the soil hydraulic properties were identical to those 10 to 20 m to the south, where unsaturated hydraulic conductivity was determined in situ from an instantaneous profile test (Hillel 1980). The two sites are within the same geologic map units (Machette 1978); and Leavitt (1986) found no statistically significant difference in hydraulic properties within the map units at the Sevilleta site. Nevertheless, there is uncertainty in the calculated flux due to the hydraulic conductivity water content relationship, as discussed for this soil by Stephens and Knowlton (1986). They found that the 95% confidence interval about conductivity was ± 19% at 0.075 cm^3/cm^3 water content.

Another likely source of uncertainty in calculating fluxes is the error in the pressure head gradients. These errors are from two distinct sources: one is the error in measuring the pressure in the tensiometer, and the other is the actual distance between pressure head measurements. The first type of error is the one made in measuring the pressure inside the tensiometer by a tensimeter (portable pressure transducer). According to the manufacturer, the tensimeter reading is accurate to ± 1 millibar, or about 1 cm of water. Tensiometers which are designed to be used with a portable pressure transducer are very sensitive to changes in temperature. For example, at the beginning of our monitoring we observed diurnal temperature change of up to about 80 cm over an air temperature change of about 25°C (Figure 11). Pressure head measurements were taken just before sunrise in order to minimize the temperature effect. About an hour was required

to collect all pressure head data, and during this time the air temperature would change. Moreover, solar radiation would heat the air inside the tensiometers. Since field measurements suggested that temperature affects all tensiometers equally, it was considered reasonable to compute pressure head gradients only when measurements were collected at about the same time and under the same temperature conditions. Within a group of vertically nested tensiometers, pressure head was measured at nearly the same time. Therefore, the error in vertical gradient calculations made using data from one tensiometer nest should be very small. Measurements taken from adjoining nests which were used to compute horizontal flux may be separated by enough time that mean pressure head between nests may differ by an estimated 1.7 cm of water, based on field observations. However, the error could be more, perhaps at least 3 cm (Hicks 1990).

Another likely source of error in pressure head gradients is due to the location of the tensiometers. The distance between pressure head measurements must be known to calculate the gradient. As mentioned previously, a surveyor's level was used to set the tensiometer cup to a particular depth below a datum. The datum was surveyed from a township marker to a stake which marked the center of each tensiometer nest. For this reason, the error in the vertical direction is small, perhaps about 0.5 cm, but the separation distance between the tensiometers in a nest is also small, only 30 cm. The horizontal separation of the tensiometers is known with less certainty. It was very difficult to drive the tensiometer insertion tool into the soil while keeping it truly vertical. A small inclination at the top of the rod will cause the tensiometer cup to be progressively farther off true vertical the deeper it is placed. An estimate of ± 2 cm was used for the error associated with the horizontal placement of tensiometer.

Finally, the magnitude of the error in the calculated flux depends on the soil's water content. This error is in addition to the uncertainty in the water content measurements made with a neutron probe, and the uncertainty in the relationship between conductivity and water content due to methodology or spatial variability. Since flux is the product of the gradient and the hydraulic conductivity (Equations 2 and 3), the error in calculated flux also increases with the soil's water content, as illustrated in Table 5. The magnitude of error in the flux calculations due to uncertainty in calculating the pressure head gradient varies from 3.93×10^{-5} cm/day at 0.03 cm^3/cm^3 moisture content to 2.1×10^{-4} cm/day at 0.03×10^{-5} cm/day at 0.03 cm^3/cm^3 moisture content to 2.1×10^{-4} cm/day at 0.05 cm^3/cm^3 moisture content. By comparison, the

TABLE 5. Error in fluxes due to uncertainty in pressure head gradients at 0.03, 0.04, and 0.05 cm^3/cm^3 volumetric water content.

Lateral fluxes and vertical fluxes are shown in (a) and (b), respectively, and are based on an average pressure head of a -100 cm water.

(a) Lateral Fluxes

WATER CONTENT (cm^3/cm^3)	ERROR IN GRADIENT (cm/cm)	CONDUCTIVITY (cm/day)	MAGNITUDE OF FLUX ERROR (cm/day)
0.03	0.541	7.26×10^{-4}	3.93×10^{-5}
0.04	0.541	1.67×10^{-3}	9.03×10^{-5}
0.05	0.541	3.88×10^{-3}	2.10×10^{-4}

(b) Vertical Fluxes

WATER CONTENT (cm^3/cm^3)	ERROR IN GRADIENT (cm/cm)	CONDUCTIVITY (cm/day)	MAGNITUDE OF FLUX ERROR (cm/day)
0.03	0.0690	7.26×10^{-4}	5.01×10^{-5}
0.04	0.0690	1.67×10^{-3}	1.15×10^{-4}
0.05	0.0690	3.88×10^{-3}	2.68×10^{-4}

horizontal fluxes calculated with the program are approximately 1.0×10^{-5} cm/day at the same moisture contents. During significant parts of the year, many of the lateral fluxes are not larger than the expected error in their calculations, and the computed values could be the result of experimental error.

However, because some of the horizontal fluxes are sufficiently large relative to the errors described above, there is some confidence that they are indeed significant. For example, Figure 16 shows the fluxes across the west face of cell, one which is closest to the line of four-wing saltbush. July 1988 data show flux west toward the bush at all depths, with most

values in excess of 10^{-4} cm/day. After the heavy rains of August and September of that year, the pattern changed such that either most of the flux reversed direction to the east, away from the saltbush, or became smaller in magnitude in the westward direction. During June and July 1989, most of the horizontal flux components were again west in the direction of the saltbushes. Although the magnitude of lateral flux seems significant, the reversals in flow direction seen in the current study are difficult to explain. As observed by Kickham (1987), plant roots seem to be dynamic and extract moisture from different parts of the soil during the season.

Moisture Content Analysis

Analysis of the moisture distributions throughout the study period also offer insights into seasonal and spatial variabilities in soil-water movement. Moisture content reveals information about moisture losses and gains caused by infiltration, evaporation, and redistribution.

Figure 19 shows moisture content profiles at two locations, neutron probes 6 and 11 (Figure 5), during the summer and winter. It is evident that the two moisture-content profiles are very similar over depth and time. These profiles illustrate the soil's uniformity and its response to infiltration. The greatest seasonal variations in moisture contents are detected in the upper 90 cm and lower 300 cm of soil.

Moisture content changes in the upper 90 cm are attributed to late summer rains. Figure 20 shows moisture-content distributions before and after a period of heavy precipitation. During this period, July 20, 1989 to August 8, 1989, a total of 3.7 cm of rain was recorded, and moisture content increases were evident in the upper 60 cm of the soil profile. From August 6, 1988 to October 10, 1988, precipitation totaled 8.3 cm and the wetting front propagated to a depth of about 60 cm near the saltbush canopy and to almost 90 cm near the center of the plot (Figure 21). However, Stephens et al. (1985) found that wetting front propagated to more than 2 m in the fall and winter of 1984-85 when more than 10 cm of precipitation occurred very near this site at a time when evapotranspiration was minimal.

The seasonal variation in moisture content observed below 300 cm is due to fluctuations in water table elevation. During the late summer rainy season, the Rio Salado, the ephemeral stream located approximately 25 m north of the field site, commonly flows for periods of days to

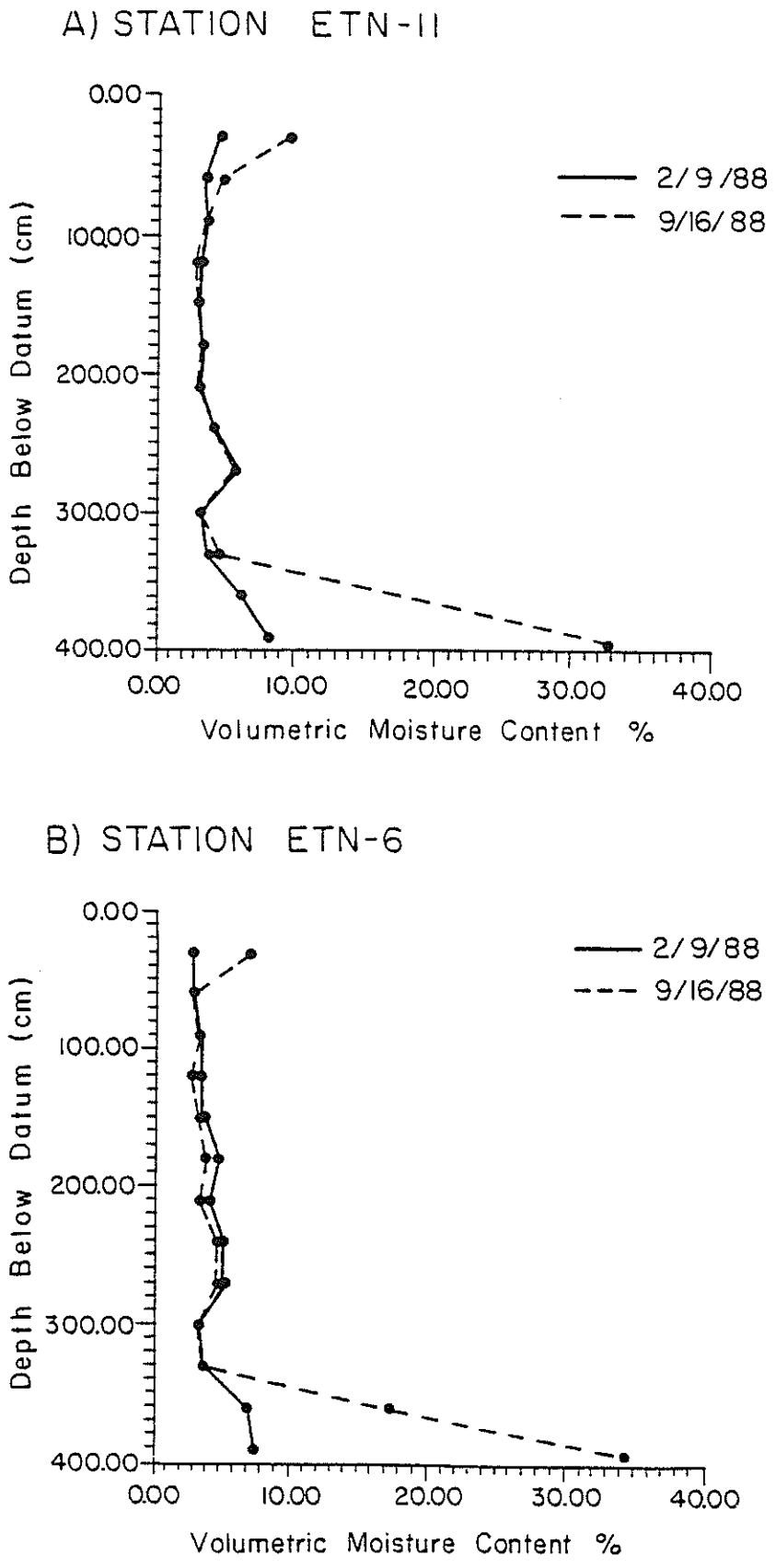

FIGURE 19. Moisture-content profiles in winter and summer 1988.

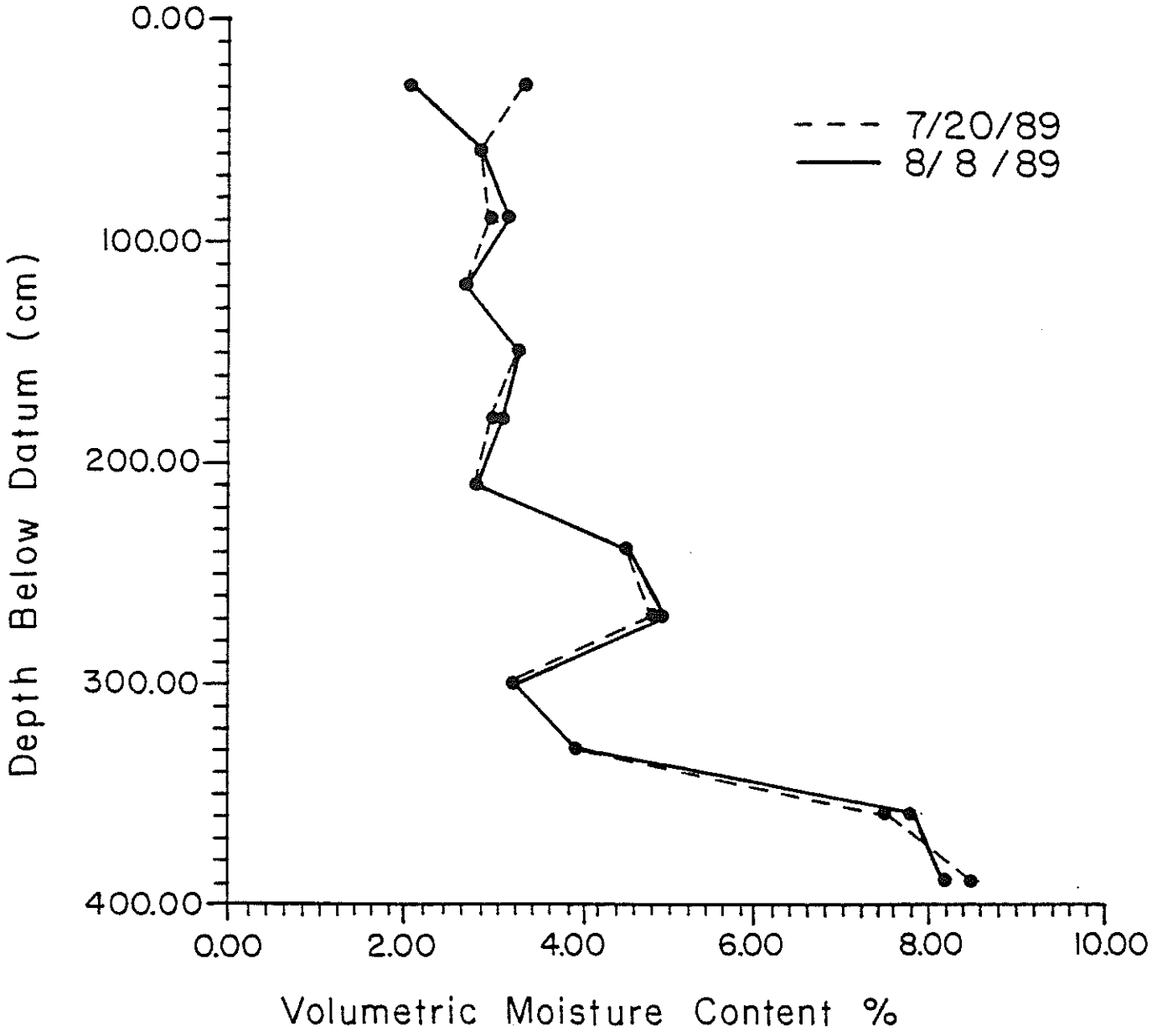

FIGURE 20. Moisture-content profile at ETN-1 in summer 1989. Total precipitation between logging dates was 3.7 cm.

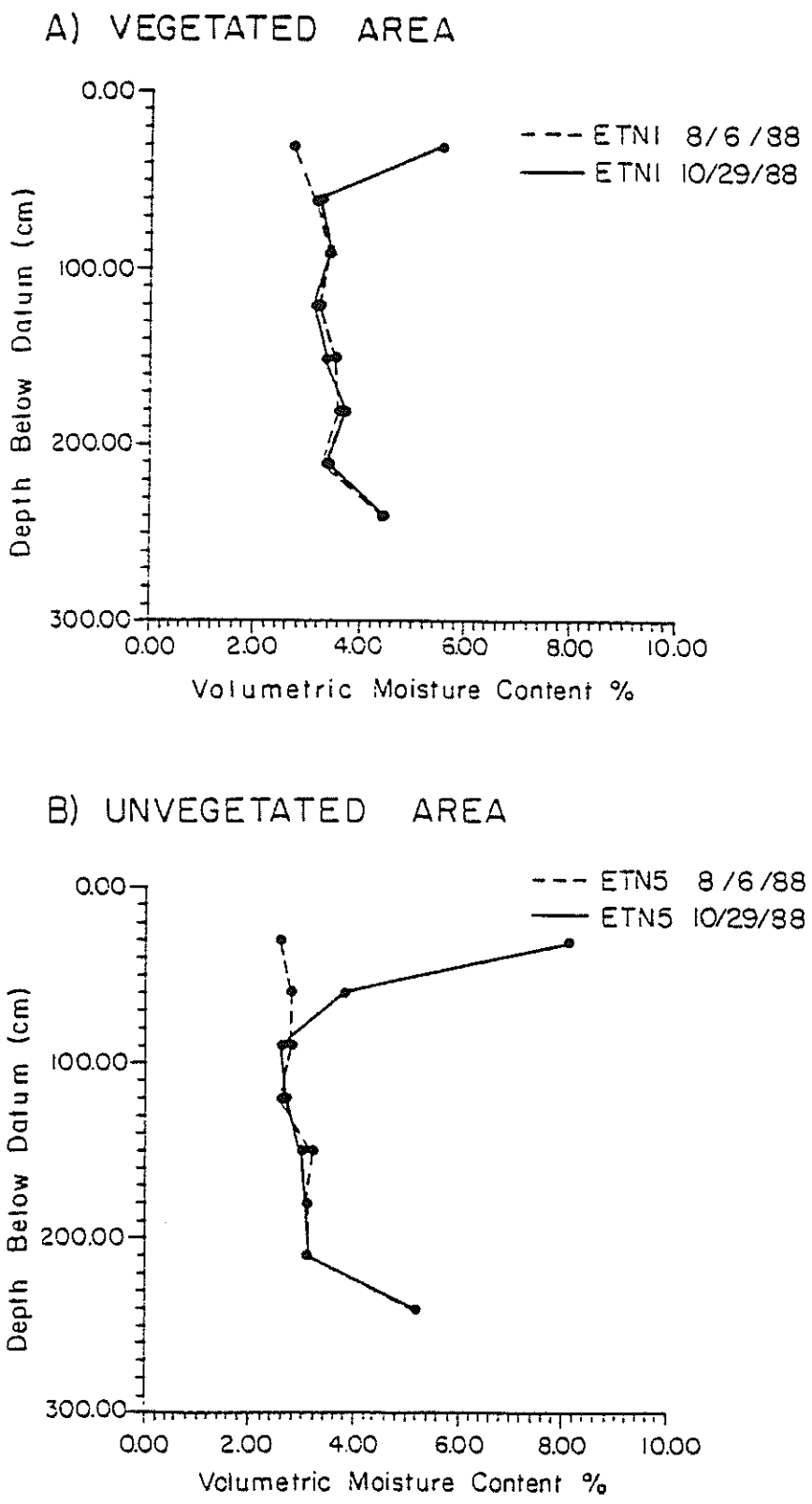

FIGURE 21. Moisture-content profile at (a) vegetated and (b) unvegetated parts of plot, August 8 and October 29, 1988. Total precipitation between logging dates was 8.3 cm.

weeks. During this time, the stream is hydraulically connected to the alluvial aquifer and, as a result, the water table slowly rises in response to runoff. In the study by Stephens et al. (1988), the water table beneath the site fluctuated by as much as a meter due to recharge from the Rio Salado. Between 60-300 cm the moisture-content profiles from the two locations within the site are very similar. There is little evidence of significant seasonal variations in moisture content within this interval. Within this depth interval the moisture content is about 3% to 4%, except at the 270 cm depth where the moisture content increases to about 5% to 6% due to a silty layer (Figure 6). Figures 22 and 23 illustrate the spatial distribution in vertical sections before and after runoff in the Rio Salado. The effect of the water table rise is readily apparent.

An important feature of the cross sections in Figures 22 and 23 is that there is little evidence of horizontal variability in moisture content at a time when one might expect plant root extraction to be at a maximum. This may be attributed to the absence of significant spatial variability in root distribution (Figure 8). However, large woody roots were encountered in some borings at depths of 4 m near the plot's center. It is entirely possible that most of the water used by the saltbush is derived by tap roots which penetrate to the water table. Recall that there was also little seasonal variability in moisture content at a given location, which supports the notion that a tap root beneath the canopy, rather than lateral root systems, may provide most of the plant's moisture. Alternatively, the root system of the saltbush may be so fine, uniform, and extensive already, that significant changes in water content are not measurable with the neutron probe for this soil. At low-water contents, such as at our site, water flow to roots could occur without affecting a measurable change in water content by the neutron probe, owing to the large values of $dK/d\theta$ (steep K-θ curve) which are typical of this and other relatively coarse-textured soils. The depleted soil moisture may be quickly replenished by only small recharge fluxes. Consequently, the soil moisture regime may appear to be in a state of dynamic equilibrium in this depth interval. The latter alternative is supported by Dwyer and DeGarmo (1970) who found that relative to mesquite and creosote, saltbush required the least water to produce a gram of plant matter and it had the most uniform root distribution. They also noted that in dry soils, saltbush roots tend to be much finer than under wetter conditions.

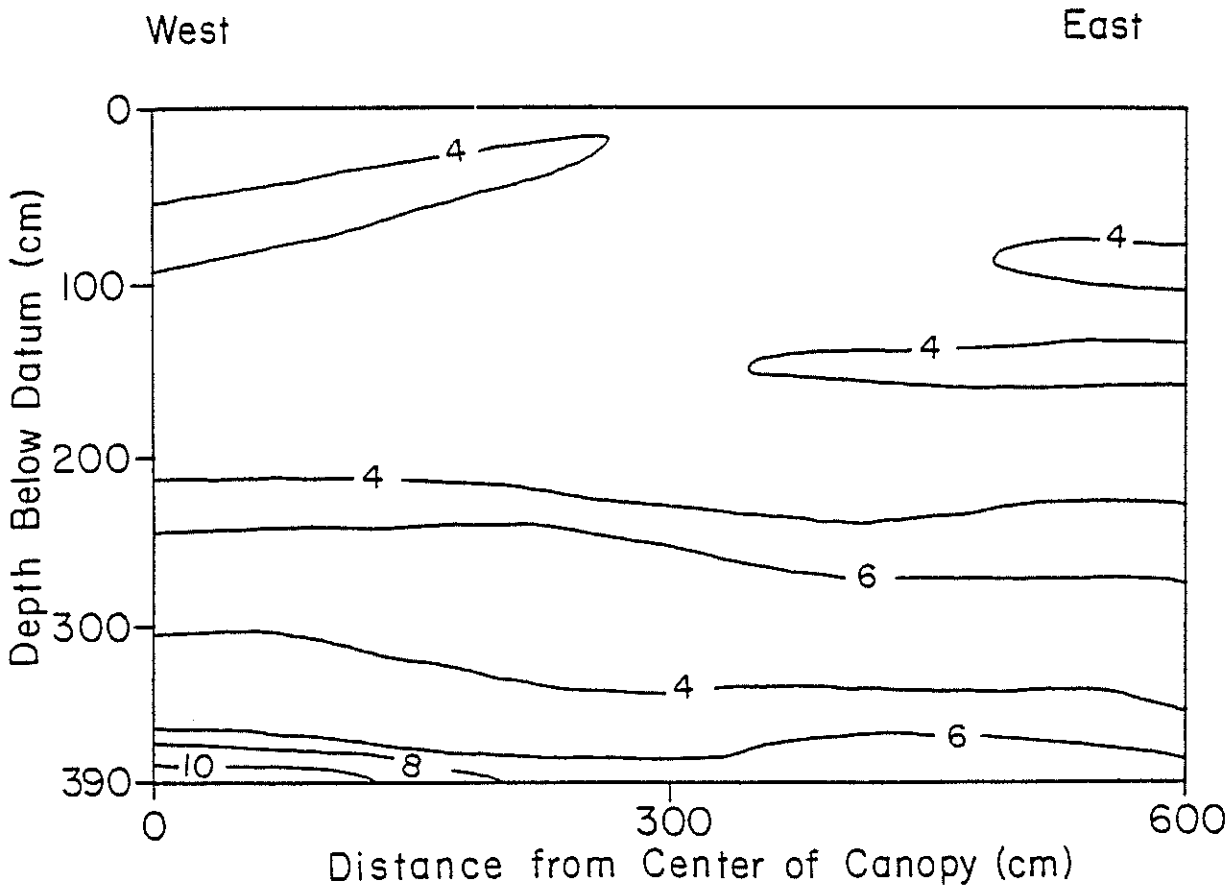

FIGURE 22. Moisture-content (percent by volume) cross-section on August 20, 1988 from neutron probe access tubes ETN 2, 5, 8, and 11.

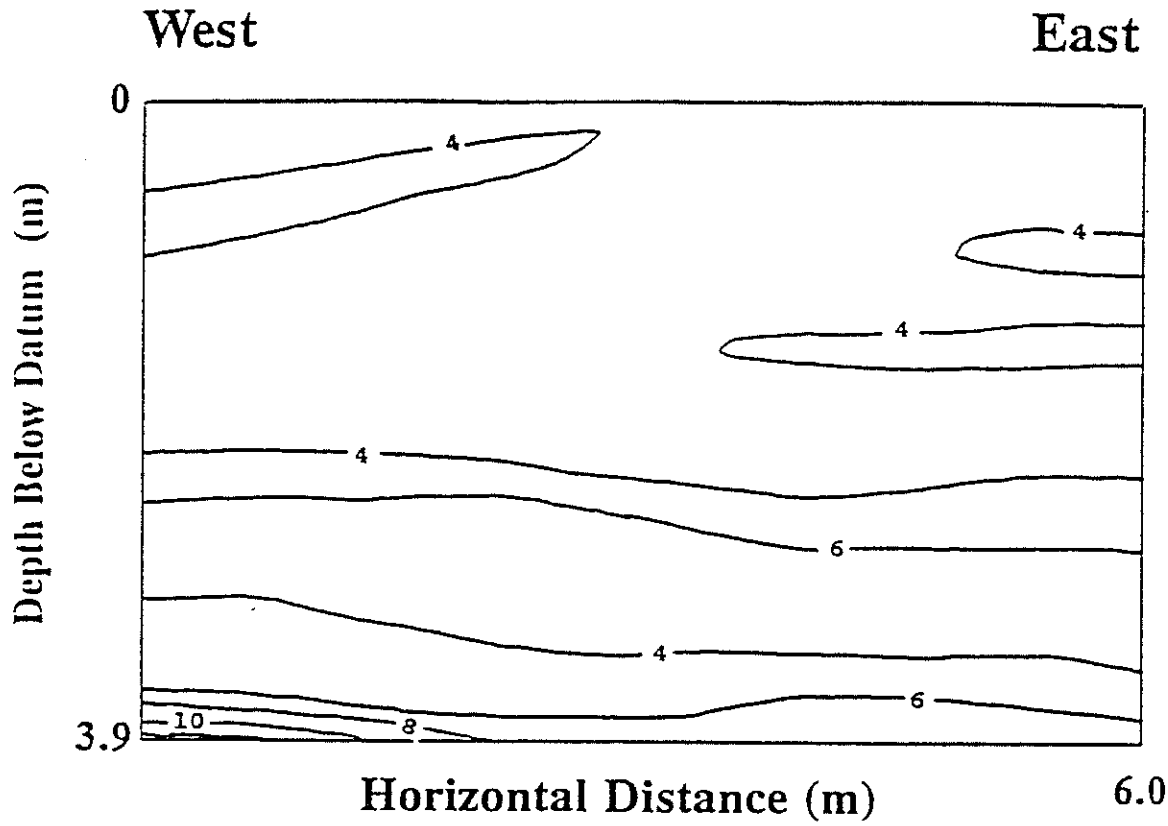

FIGURE 23. Moisture-content cross section on September 16, 1988 from neutron probe access tubes ETN 2, 5, 8, and 11, subsequent to water table rise.

Soil-Water Tracers

Figures 24 and 25 show the plumes of bromide and 2,6-DFBA which developed after 169 days. Recall that the bromide source was 30 cm deep and the organic acid source was 90 cm deep. During this period, August 9, 1988 to January 24, 1989, precipitation was about 10.6 cm. The center of bromide mass was displaced vertically downward approximately 7.5 cm in the westerly location near the shrubs and about 48 cm in the easterly location near the less vegetated central part of the plot. By comparison, the 2,6-DFBA moved about 5 cm upward near the vegetation and about 17 cm downward in the central part of the plot. Local upward gradients were calculated for portions of the plot (Hicks 1990) and are not unexpected near roots. Because of uncertainty in the precise depths of tracer emplacement and soil sampling, depths of tracer concentration are probably accurate only to within ± 5 cm. Additionally, the tracer concentration is averaged over about a 5 cm length of core. Consequently, the conclusion that soil-water movement may be upward, at least locally, is subject to cnosiderable uncertainty due to measurement errors.

In general, the tracers do confirm that the principal direction of soil-water movement is vertical at this plot. The tracer data suggest that water movement downward is most rapid at shallow depths where moisture content and hydraulic conductivity may increase significantly following precipitation. The downward percolation at shallow depths (within about 0-30 cm) is also enhanced by relatively low capillary pressure ahead of the advancing wetting front. Note that the bromide plume significantly overlaps the 2,6-DFBA plume. The depth of tracer penetration to about 100 or 125 cm extends deeper than the zone where significant soil-water content changes were measured during this time (Figure 21).

The tracer data also suggest that downward soil-water movement is influenced by vegetal cover. Greater depths of tracer penetration near the less vegetated part of the plot suggest that greater infiltration and recharge occur where vegetation density is lowest. This result is not entirely consistent with soil water-fluxes evaluated for the six zones (Figure 5) from the hydrodynamic measurements (Table 3). The reasons for this inconsistency are not understood at this time. Nevertheless, the tracer plumes clearly show that the liquid phase is continuous at the field moisture content. This is important because some scientists believe that vadose zone transport virtually ceases whenever the moisture content reaches so-called "field capacity." We

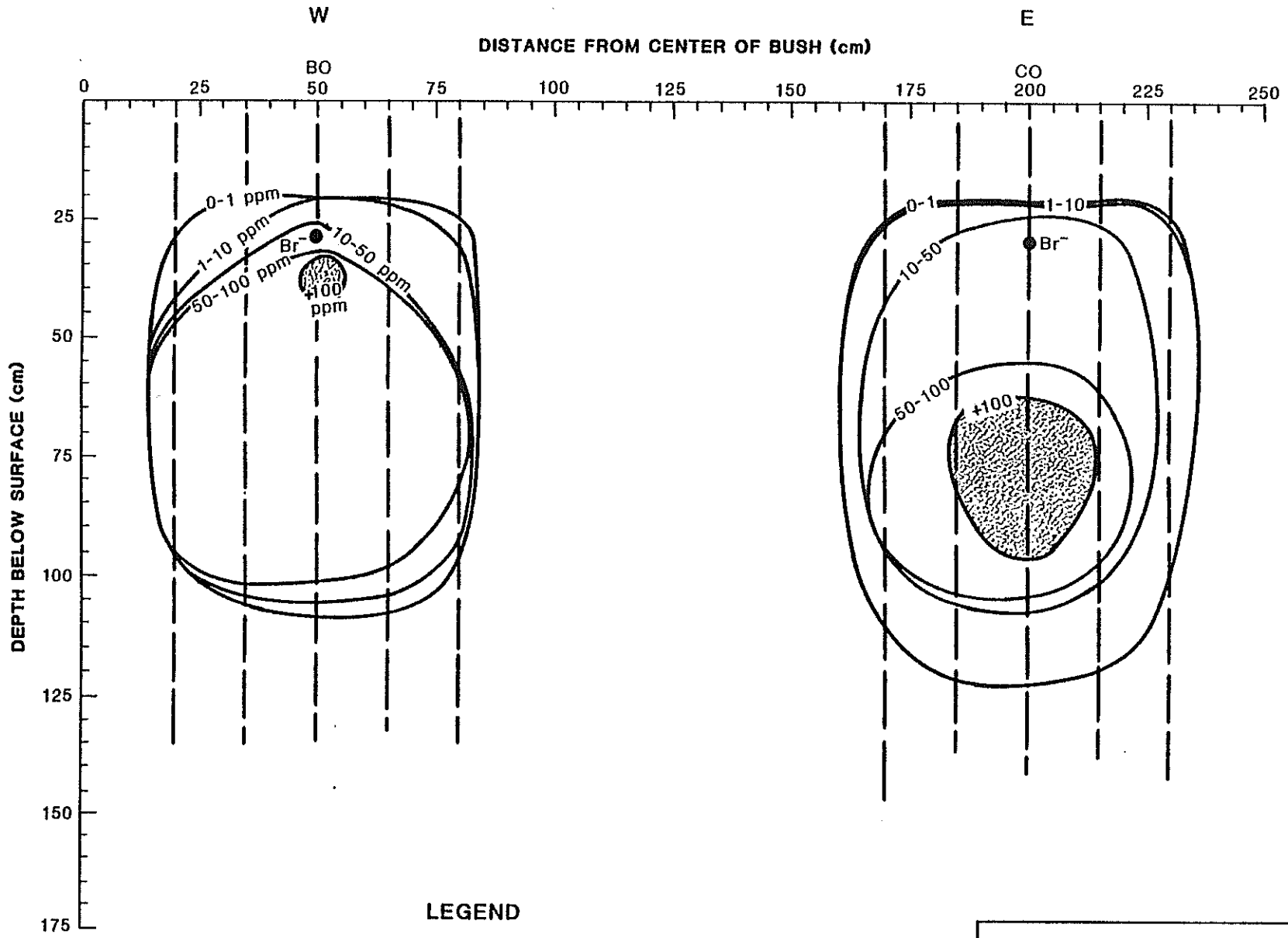

FIGURE 24
SOLUTE PLUME CONTOURS OF BROMIDE

DATE	PROJECT NO	DESIGNED BY	DRAWN BY	CHECKED BY

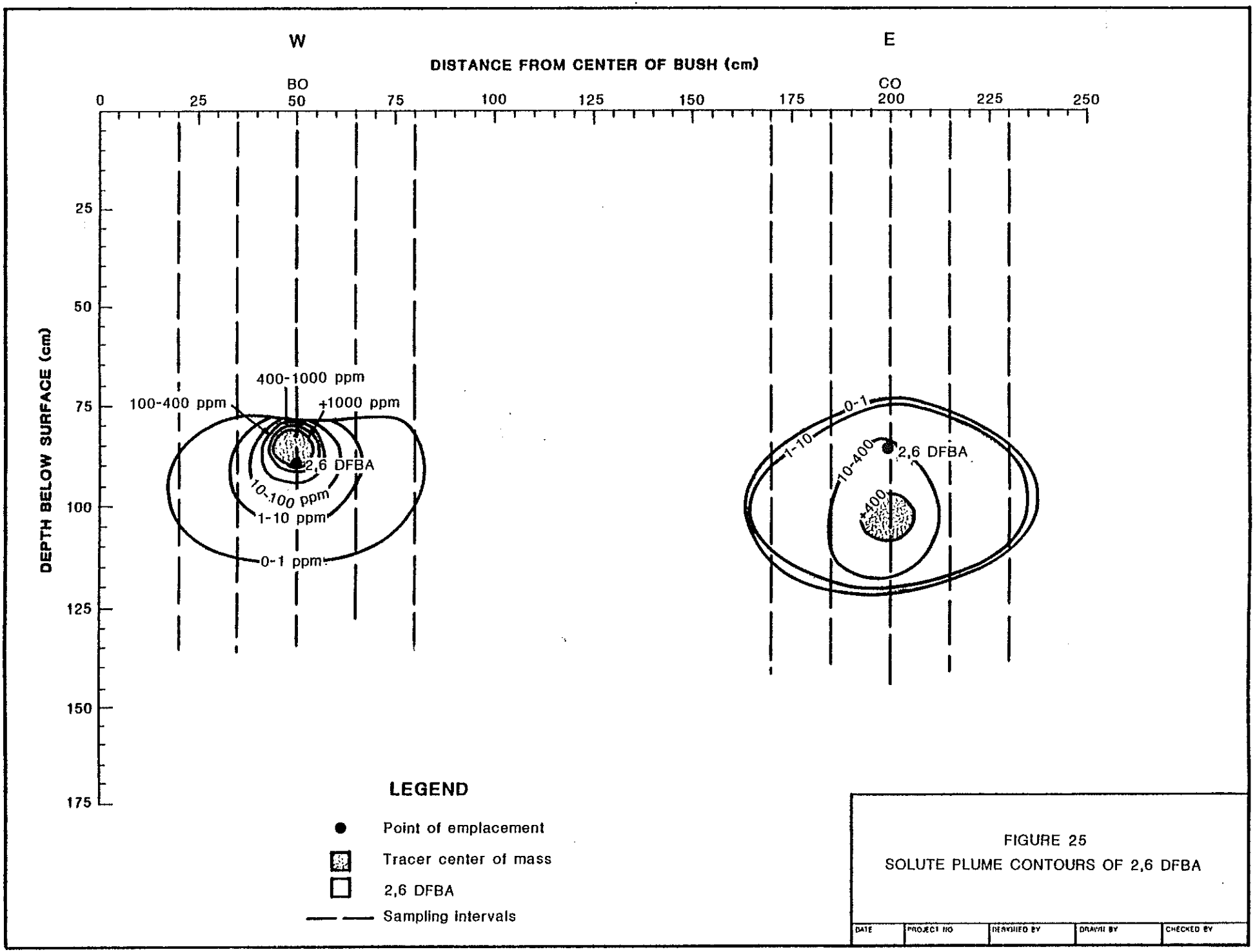

FIGURE 25
SOLUTE PLUME CONTOURS OF 2,6 DFBA

DATE	PROJECT NO	DESIGNED BY	DRAWN BY	CHECKED BY

observed very little moisture content change below depths of about 80 cm (Figures 19, 20, and 21), where moisture content averaged about 3.5% (Stein 1990). In spite of the low water content and the fact that annual potential evapotranspiration far exceeded precipitation, soil water moved downward in the central part of the plot. If we assume that the linear velocity of 2,6-DFBA is 0.103 cm/day (17.5 cm/169 days) and the mean volumetric moisture content is 3.5%, than the Darcy velocity or recharge flux would be about 0.9 cm/yr. This recharge is, in general, in agreement with the hydrodynamic results described earlier.

The tracer tests also reveal a plume shape which is symmetric but elongated more in the horizontal than in the vertical direction. We infer from this observation that transverse dispersion is greater than the longitudinal dispersion. Such a result is not widely expected, although recent work by Kung (1988) described similar field results with dye tests. Apparently, fine scale stratification contributes significantly to anisotropy in dispersivity under unsaturated flow conditions, and this finding may have broader implications for modeling contaminant transport in the vadose zone.

Soil-Water Balance

Based upon the precipitation record, recharge calculations, and moisture content changes in the profile, we computed a water balance over the period of record July 5, 1988 to July 20, 1989 (Equation 5). During this 381-day period, the annual precipitation rate was 17.4 cm/yr. Average soil moisture over the 12 neutron probes increased at an annual rate of 3.3 cm/yr in the depth interval of 30 to 240 cm. The ground-water recharge (i.e., discharge from the profile) was computed from the mean flux using field measured hydraulic conductivity at in situ moisture and hydraulic gradient between 210 and 240 cm depths. The mean annual recharge over all six cells in the plot was 0.4 cm/yr. Soil moisture evapotranspiration, represented by the residual from Equation 5, is therefore 13.7 cm/yr. Based on the annual precipitation, soil-moisture storage represents 18.9% of precipitation, recharge from percolation through the soil represents 2.3% of precipitation and soil moisture evapotranspiration comprises 78% of precipitation. Actual evapotranspiration may be much greater than evapotranspiration from the vadose zone, because some roots may withdraw water from the shallow aquifer. Roots may also extract some moisture that percolates below 240 cm; consequently, our recharge estimates may be high.

The soils at the site of our water balance study are in the Blue Point series which are mixed, thermic Typic Torripsamments. This soil map unit occurs over significant parts of Socorro County. Although recharge from soil-water percolation is a small portion of precipitation, it cannot be neglected for ground-water management purposes in low precipitation areas. For example, for each 1000 acres, a recharge rate of 2.3% of precipitation (17.4 cm/yr) would contribute 75 acre-feet per year, or 46 gallons per minute to ground water. Such yields are indeed important to our long-term water resources planning.

It is important to recognize that some recharge to the shallow aquifer occurs by other processes, such as stream channel infiltration. In the water balance of a larger spatial domain, one would need to consider stream channel infiltration, water table fluctuations (ground water storage), and actual evapotranspiration components.

Comparison of Methods to Compute Recharge

It is important to recognize that the hydrodynamic approach used here to compute recharge reflects recharge rates only for the period of measurement. There can be significant variability in recharge from one year to the next, as suggested by a comparison of the results of our study with those from Stephens and Knowlton (1986). In the latter study, at a fluvial sand plot about 20 m south of the current investigation, the recharge was as much as 3.7%, or more, of precipitation from November 1982 to May 1984 when precipitation averaged 17.7 cm/yr. This is about the same as precipitation during our study. Greater recharge may occur when precipitation is greater and when more precipitation occurs in winter. For instance, the 30-year mean precipitation (1941 to 1970) at Socorro is about 20 cm, which is slightly greater than that measured at our site.

Chlorine-36 and tritium, which are derived from thermonuclear weapons tests, are often excellent long-term tracers of soil water movement. Only about 20 m east of our plot, in the same sand facies, Phillips et al. (1988) found that chlorine-36 and tritium analysis give recharge rates which are approximately 0.3 to 0.8 cm/yr for this site (Phillips et al. 1988). Such long-term rates are remarkably similar to the recharge rate of 0.4 cm/yr we calculated by hydrodynamic methods and 0.9 cm/yr from the 2,6-DFBA tracer near the center of the plot. The similarity in results of

the hydrodynamic and tracer tests compared with the isotopic methods gives us confidence that our results are very reasonable.

It must be noted that the deep soil-water flux which becomes recharge over the year is the result of precipitation from that year as well as from previous years. Consequently, it is not entirely appropriate to express annual recharge as a percentage of annual precipitation. From our limited data base, it is not possible to determine the proportions of specific precipitation events, or the years of precipitation, which actually reached the water table during our field measurements.

SUMMARY OF CONCLUSIONS

1. Significant three-dimensional soil moisture flow patterns were not observed in the immediate vicinity of a saltbush community. Calculated horizontal flux components were of the same magnitude as the error in the computation.

2. During the period of record, July 1988 to July 1989, below about 90 cm and above 300 cm, field instrumentation and monitoring data show that the soil-water content was nearly constant and the hydraulic gradient downward was nearly unity.

3. Within the six instrumented 2.25 m^2 zones of the plot, recharge calculated by hydrodynamic methods was spatially variable, ranging from about 0.16 to 1.02 cm/yr. The mean recharge from the six zones was about 0.4 cm/yr. Precipitation during this time was approximately 17.4 cm although, uncharacteristically, little of this occurred in winter.

4. Bromide and 2,6-DFBA tracers, from within at least the upper 125 cm of the central part of the plot, suggest that flow is vertically downward; however, at the 90 cm depth near the shrubs, net upward flow of tracer has occurred during the 169 day experiment.

5. The amount of 2,6-DFBA tracer displacement near the center of the plot is consistent with a recharge rate of about 0.9 cm/yr.

6. Recharge rates calculated at this site by hydrodynamic methods are in very good agreement with independent results using tritium and chlorine-36 at a nearby location.

7. Within the soil profile above the water table, about 79% of the annual precipitation was consumed by soil-water evapotranspiration, about 19% went to increase soil-moisture storage, and about 2% became recharge.

REFERENCES

Bowman, R.S., 1984, Evaluation of some new tracers for soil water studies, Soil Sci. Soc. Amer. Jour., 48:987-993.

Dwyer, D.D. and H.C. DeGarmo, 1970, Greenhouse productivity and water-use efficiency of selected desert shrubs and grasses under four soil-moisture levels, New Mexico State University Agricultural Experimental Station Bulletin, 570:1-15.

Gee, G.W; M.L. Rockhold, J.L. Downs, 1989, Status of Fiscal Year 1988 Soil-Water Balance Studies or the Hanford Site, Pacific Northwest Laboratories PNL-6750, pp

Gee, G.W., and D. Hillel, 1988, Groundwater recharge in arid regions: review and critique of estimation methods, Hydrological Processes, 2:255-266.

Hicks, E.M., 1990, Estimated ground-water recharge at a naturally vegetated semiarid site from a darcian and mass balance of chloride approach, Unpublished Masters of Science Independent Study Paper, Geoscience Department, New Mexico Tech, Socorro, New Mexico.

Hillel, D., 1980, Fundamentals of Soil Physics, Academic Press, New York, 413, pp.

Kickham, B.J., 1987, A field study on the water use of a *Dalea scoparia* plant in the northern Chihuahua desert, unpublished independent study paper, New Mexico Institute of Mining and Technology, Socorro, New Mexico.

Knowlton, R.G., Jr., 1984, Field study and numerical simulation of natural ground-water recharge, Unpublished Independent Study Paper, New Mexico Institute of Mining and Technology, Socorro, New Mexico.

Kung, K.J.S., 1988, Ground truth about water flow patterns in a sandy soil and its influence on solute sampling and transport modeling, in Validation of flow and transport models for the unsaturated zone, conference proceedings, May 22-25, 1988, Ruidoso, New Mexico, P.J. Wierenga and D. Bachelet (editors), Research Report 88-55-04, Dept. Agronomy and Horticulture, New Mexico State University, Las Cruces, New Mexico..

Leavitt, M.L., 1986, Spatial variability of the hydrologic parameters of soils at Sevilleta National Wildlife Refuge, Unpublished Masters of Science Independent Study Paper, Geoscience Department, New Mexico Tech, Socorro, New Mexico.

Machette, M.C., 1978, Geologic map of the San Acacia Quadrangle, Socorro County, New Mexico, Map GQ-1415, U.S. Geological Survey, Washington, D.C.

McCord, J.T., 1986, Topographic Controls on Ground-Water Recharge at a Sandy, Arid Site, Unpublished Masters of Science Independent Study Paper, Geoscience Department, New Mexico Tech, Socorro, New Mexico.

McKim, H.L., R.L. Berg, R.W. McGaw, R.T. Atkins and J. Ingersoll, 1976, Development of a remote reading tensiometer/transducer system for use in subfreezing temperatures, in Proceedings 2nd Conference on soil-water Problems in Cold Regions, Edmonton, Alberta, Canada, 31-45.

Phillips, F.M., J.L. Mattick, and T.A. Duval, 1988, Chlorine 36 and tritium from nuclear weapons fallout as tracers for long-term liquid and vapor movement in desert soils, Water Resour. Res., 24(11):1877-1891.

Stein, T.L., 1990, Moisture movement at a desert site, Unpublished Master of Science Independent Study Paper, New Mexico Institute of Mining and Technology, Socorro, New Mexico.

Stephens, D.B., W. Cox and J. Havlena, 1988, Field Study of ephemeral stream infiltration and recharge, Technical Completion Report, Project No. 1423655, New Mexico Water Resources Research Institute, Las Cruces, New Mexico, 182 pp.

Stephens, D.B., and R.G. Knowlton, Jr., 1986, Soil-water movement and recharge through sand at a semiarid site in New Mexico, Water Resour. Res., 22(6):881-889.

Stephens, D.B., R.G. Knowlton, Jr., J.T. McCord, and W. Cox, 1985, Field Study of Natural Ground-Water Recharge in a Semiarid Lowland, Technical Completion Report, Project No. 1345679, New Mexico Water Resources Research Institute, Las Cruces, New Mexico, 91 pp.

Stephens, D.B., S.P. Neuman, S. Tyler, K. Lambert, D.Watson, R. Knowlton, Jr., E. Byers, and S. Yates, 1983, In situ determination of Hydraulic Conductivity in the Vadose Zone using Borehole Infiltration Tests, Technical Completion Report, Project B-0703-NMEX, New Mexico Water Resources Research Institute, Las Cruces, New Mexico, 165 pp.

van Genuchten, M. Th., 1980, A closed-form equation for predicting the hydraulic conductivity of unsaturated soils, Soil Sci. Soc. Amer. Proc., 44(5):892-898.

Wendt, C.W., O.C. Wilke and L.L. New, 1978, Use of methanol-water solutions for freeze protection of tensiometers, Agronomy Journal, 70:890-891.

APPENDIX

```
**************************************************************
This program calculates flux through each face of the
computational cells at the field site using Darcy's law.
Required input is water content of the soil and pressure head
measurements. This data is stored in a separate file which the
user specifies during the execution of the code. From pressure
head data hydraulic gradients are calculated. Unsaturated
hydraulic conductivities are derived from a field determined
relationship between volumetric water content and unsaturated
hydraulic conductivity. The time span over which the pressure
head and moisture content values are believed to be
representative must be entered if change in water storage is
to be calculated. The change in storage of water in each cell
is calculated by summing the product of the flux through each
face by that face's surface area and the time that flux
occurred.

**************************************************************

C Declaration of variables

 implicit real*8 (a-h,o-z)
 dimension theta(1:4,1:3,1:8), psi(1:5,1:4,1:8),
/flux(1:6,1:5,1:6), cellstor(1:6,1:5)

 integer depth, cell, i, j, k, l, m, n
 character infil*50,outfil*50
 logical failed

C ******** Variable Dictionary ****************************

* theta    3-d array containing water content data

* psi      3-d array containing pressure head values

* flux     3-d array containing flux through each face of cell

* cellstor 2-d array containing change in storage of water for
*          each cell at site

* depth    Interval of cell ( which slice of cell 1 through
*          6 is being considered ) See Figures 14 and 15 of
*          text.

*           Depth 1  60 to 90 cm interval
*           Depth 2  90 to 120 cm interval
*           Depth 3  120 to 150 cm interval
*           Depth 4  150 to 180 cm interval
*           Depth 5  180 to 210 cm interval

* cell     Counter which records which computational cell is
*          being considered. Ranges from 1 to 6.

* infil    Name of input file name.
```

```
* outfil   Output file name.

* failed   Logical flag for success or failure in calculating
*          change in storage of cell.

* wcav     Average water content in soil plane, determined by
*          averaging 4 water content measurements.

* cd       Unsaturated hydraulic conductivity determined by
*          placing wcav into field derived formula.

* delh     Pressure head gradient, determined from pressure
*          head data.


* i        Index used to denote x direction of pressure head
*          values. (column)

* j        Index used to denote y direction of pressure head
*          values. (row)

*          I and J values are x and y coordinates of the
*          tensiometer nests when seen in plan view. Nest
*          number one has values of (1,1) and tensiometer
*          nest number twenty has values of (5,4).

* k        Index which always indicates depth of pressure
*          head data. K = 1 for 30 cm and k = 8 for 240 cm.

*         Example: Pressure head reading for tensiometer nest
*          2, 60 cm depth is stored in psi(i,j,k)
*          i = 1 ( nest in first column )
*          j = 2 ( nest in 2nd row )
*          k = 2 ( 60 cm depth, k = 2 )

* l        Index used to denote x direction of water content
*          values. (column)

* m        Index used to denote y direction of water content
*          values. (row)

*          L and M values are x and y coordinates of the
*          water content values when seen in plan view.
*          Neutron probe access hole number one has values
*         of (1,1) and access hole number twelve has values
*         of (4,1).

* n        Index which always indicates depth of moisture
*          content reading. L = 1 for 30 cm and l = 8 for 240
*          cm.
*****************************************************************
*****************************************************************
```

```
* Ask the user for input and output file names ************

 write(*,*)'Enter the Input File Name'
 read(*,'(a)')infil
 open(unit=99,status='old',file=infil)

 write(*,*)'Enter the Output File Name'
 read(*,'(a)')outfil
 open(unit=98,status='unknown',file=outfil)

* Ask user for time data is valid ***************************
 write(*,*)'Enter the Number of Days Flux in Effect'
 read(*,*)days

C Read in moisture content data ******************************
* Must be in following order: 1, 2, 3, 6, 5, 4, 7, 8, 9, 12,
* 11, 10, eight values per line starting with 30 and ending
* with 240 cm.

 do 10 i = 1,4
   do 20 j = 1,3
       read(99,*)(theta(i,j,k), k = 1,8)
 20   continue
 10   continue

C Read in the pressure head values ***************************
* Must be in the following order: 1, 2, 3, 4, 8, 7, 6, 5, 9,
* 10, 11, 12, 16, 15, 14, 13, 17, 18, 19, 20 eight values per
* line starting with 30 and ending with 240 cm. Missing
* pressure head data should be indicated in the data files by
* a positive number as a flag for the program, not blanks.


 do 30 i = 1,5
    do 40 j = 1,4
        read(99,*)(psi(i,j,k), k = 1,8)
 40    continue
 30 continue

************************************************************
C Calculations ***********************************************

* Start with first cell ***
 cell = 1

* Start x counter for pressure head ***
 do 50 i = 2, 4

*  Initialize x counter for water content ***
   l = i-1

* Start y counter for pressure head ***
   do 60 j = 2, 3
```

```
*     Initialize y counter for water content ***
      m = j-1

*     Start depth counter for pressure head ***
      do 70 k = 2, 6

*       Set depth counter for water content ***
        n = k

*       Set depth of cell counter ***
        depth = k-1

*      Initialize all storage values to zero and failed is not
*       true yet
        cellstor(cell,depth) = 0
        failed = .false.

*************************************************************
C Flux through the western face  ****************************

* Calculate average water content of face *****
 wcav =(theta(1,m,n)+theta(1,m+1,n)+theta(1,m,n+1)+
/theta(1,m+1,n+1))/400.0

* Calculate unsaturated hydraulic conductivity ***
 cd = 5.86656e-5 * exp(83.84*wcav)

* Calculate gradient ****************************************
* Positive delh means flux into the cell ***
 delh =((psi(i-1,j,k)+psi(i-1,j,k+1))/2.0-(psi(i,j,k)+
/psi(i,j,k+1))/2.0)/150.0

* Handle missing pressure head data ************************
* Positive psi values indicate missing data **

* Use k + 1 value if k missing ***
 if (psi(i-1,j,k ) .gt. 0) then
     delh = (psi(i-1,j,k+1)-(psi(i,j,k)+psi(i,j,k+1))/2.0)
/    /150.0
 endif

* Use k value if k + 1 missing ***
 if (psi(i-1,j,k+1) .gt. 0) then
     delh =(psi(i-1,j,k)-(psi(i,j,k)+psi(i,j,k+1))/2.0)
/   /150.0
 endif

* Use k + 1 value if k missing ***
 if ( psi(i,j,k) .gt. 0 ) then
     delh =((psi(i-1,j,k)+psi(i-1,j,k+1))/2.0-psi(i,j,k+1))
/    /150.0
 endif

* use k value if k + 1 missing ***
```

```
 if (psi(i,j,k+1) .gt. 0 ) then
     delh =((psi(i-1,j,k)+psi(i-1,j,k+1))/2.0-psi(i,j,k))
/    /150.0
 endif

* Both k and k + 1 missing, set delh = 0 ***
 if (psi(i-1,j,k).gt.0 .and. psi(i-1,j,k+1).gt.0 ) then
     delh = 0
 endif

* Both k and k + 1 missing, set delh = 0 ***
 if (psi(i,j,k).gt.0 .and. psi(i,j,k+1).gt.0 ) then
     delh = 0
 endif


* Calculate flux by multiplying cd and delh ***
 flux(cell,depth,1) = cd * delh

* Calculate volume per time (flux times area of face)
 temp = flux(cell,depth,1) * 4500.0

* Cumulative volume of water in or out of cell ***
 cellstor(cell,depth) = cellstor(cell,depth) + temp * days

* Set flag if unable to determine delh and consequently unable
* to determine change is storage for this cell ***
 if (abs( delh - 0.0) .lt. 1.0e-24 ) then
     failed = .true.
 endif

*****************************************************************
C Flux through the eastern face ***************************

* Calculate average water content of face *****
 wcav =(theta(l+1,m,n)+theta(l+1,m+1,n)+theta(l+1,m,n+1)+
/theta(l+1,m+1,n+1))/400.0

* Calculate unsaturated hydraulic conductivity ***
 cd = 5.86656e-5 * exp(83.84*wcav)

* Calculate gradient ****************************************
* Positive delh means flux into the cell ***
delh =((psi(i+1,j,k)+psi(i+1,j,k+1))/2.0-(psi(i,j,k)+
/psi(i,j,k+1))/2.0)/150.0

* Handle missing pressure head data ************************
* Positive psi values indicate missing data ***

* Use k + 1 value if k missing ***
 if (psi(i+1,j,k ) .gt. 0) then
     delh = (psi(i+1,j,k+1)-(psi(i,j,k)+psi(i,j,k+1))/2.0)
/    /150.0
 endif
```

```
 * Use k value if k + 1 missing ***
  if (psi(i+1,j,k+1) .gt. 0) then
      delh =(psi(i+1,j,k)-(psi(i,j,k)+psi(i,j,k+1))/2.0)
/     /150.0
  endif

 * Use k + 1 value if k missing ***
  if (psi(i,j,k) .gt. 0) then
      delh =((psi(i+1,j,k)+psi(i+1,j,k+1))/2.0-psi(i,j,k+1))
/     /150.0
  endif

 * Use k value if k + 1 missing ***
  if (psi(i,j,k+1) .gt. 0) then
      delh =((psi(i+1,j,k)+psi(i+1,j,k+1))/2.0-psi(i,j,k))
/     /150.0
  endif

 * Both k and k + 1 missing, set delh = 0 ***
  if (psi(i+1,j,k).gt.0 .and. psi(i+1,j,k+1).gt.0 ) then
      delh = 0
  endif

 * Both k and k + 1 missing, set delh = 0 ***
  if (psi(i,j,k).gt.0 .and. psi(i,j,k+1).gt.0 ) then
      delh = 0
  endif

 * Calculate flux by multiplying cd and delh ***
  flux(cell,depth,2) = cd * delh

 * Calculate volume per time (flux times area of face) ***
  temp = flux(cell,depth,2) * 4500.0

 * Cumulative volume of water in or out of cell ***
  cellstor(cell,depth) = cellstor(cell,depth) + temp * days

 * Set flag if unable to determine delh and consequently unable
 * to determine change is storage for this cell ***
  if (abs( delh - 0.0) .lt. 1.0e-24) then
      failed = .true.
  endif

*****************************************************************
C Flux through the northern face ***************************

 * Calculate average water content of face *****
  wcav =(theta(l,m+1,n)+theta(l,m+1,n+1)+theta(l+1,m+1,n)+
/theta(l+1,m+1,n+1))/400.0

 * Calculate unsaturated hydraulic conductivity ***
  cd = 5.86656e-5 * exp(83.84*wcav)
```

```
* Calculate gradient ****************************************
* Positive delh means flux into the cell ***
 delh =((psi(i,j+1,k)+psi(i,j+1,k+1))/2.0-(psi(i,j,k)+
/psi(i,j,k+1))/2.0)/150.0

* Handle missing pressure head data ************************
* Positive psi values indicate missing data ***

* Use k + 1 value if k missing ***
 if (psi(i,j+1,k) .gt. 0) then
      delh = (psi(i,j+1,k+1)-(psi(i,j,k)+psi(i,j,k+1))/2.0)
/     /150.0
       endif

* Use k value if k + 1 missing ***
 if (psi(i,j+1,k+1) .gt. 0) then
      delh =(psi(i,j+1,k)-(psi(i,j,k)+psi(i,j,k+1))/2.0)
/     /150.0
 endif

* Use k + 1 value if k missing ***
 if (psi(i,j,k) .gt. 0) then
      delh =((psi(i,j+1,k)+psi(i,j+1,k+1))/2.0-psi(i,j,k+1))
/    /150.0
 endif

* Use k value if k + 1 missing ***
 if (psi(i,j,k+1) .gt. 0) then
      delh =((psi(i,j+1,k)+psi(i,j+1,k+1))/2.0-psi(i,j,k))
/     /150.0
 endif

* Both k and k + 1 missing, set delh = 0 ***
 if (psi(i,j+1,k).gt.0 .and. psi(i,j+1,k+1).gt.0 ) then
      delh = 0
 endif

* Both k and k + 1 missing, set delh = 0 ***
 if (psi(i,j,k).gt.0 .and. psi(i,j,k+1).gt.0 ) then
      delh = 0
 endif

* Calculate flux by multiplying cd and delh ***
 flux(cell,depth,3) = cd * delh

* Calculate volume per time (flux times area of face) ***
 temp = flux(cell,depth,3) * 4500.0

* Cumulative volume of water in or out of cell ***
 cellstor(cell,depth) = cellstor(cell,depth) + temp * days

* Set flag if unable to determine delh and consequently unable
* to determine change is storage for this cell ***
 if (abs( delh - 0.0) .lt. 1.0e-14) then
```

```
      failed = .true.
    endif

C Flux through the southern face ******************************
 ************************************************************

* Calculate average water content of face *****
 wcav =(theta(l,m,n)+theta(l,m,n+1)+theta(l+1,m,n)+
/theta(l+1,m,n+1))/400.0

* Calculate unsaturated hydraulic conductivity ***
 cd = 5.86656e-5 * exp(83.84*wcav)

* Calculate gradient ***************************************
* Positive delh means flux into the cell ***
 delh =((psi(i,j-1,k)+psi(i,j-1,k+1))/2.0-(psi(i,j,k)+
/psi(i,j,k+1))/2.0)/150.0

* Handle missing pressure head data ************************
* Positive psi values indicate missing data ***

* Use k + 1 value if k missing ***
 if (psi(i,j-1,k) .gt. 0) then
      delh = (psi(i,j-1,k+1)-(psi(i,j,k)+psi(i,j,k+1))/2.0)
/     /150.0
 endif

* Use k value if k + 1 missing ***
 if (psi(i,j-1,k+1) .gt. 0) then
      delh =(psi(i,j-1,k)-(psi(i,j,k)+psi(i,j,k+1))/2.0)
/     /150.0
 endif

* Use k + 1 value if k missing ***
 if (psi(i,j,k) .gt. 0) then
      delh =((psi(i,j-1,k)+psi(i,j-1,k+1))/2.0-psi(i,j,k+1))
/     /150.0
 endif

* Use k value if k + 1 missing ***
 if (psi(i,j,k+1) .gt. 0) then
      delh =((psi(i,j-1,k)+psi(i,j-1,k+1))/2.0-psi(i,j,k))
/     /150.0
      endif

* Both k and k + 1 missing, set delh = 0 ***
 if (psi(i,j-1,k).gt.0 .and. psi(i,j-1,k+1).gt.0 ) then
      delh = 0
 endif

* Both k and k + 1 missing, set delh = 0 ***
 if (psi(i,j,k).gt.0 .and. psi(i,j,k+1).gt.0 ) then
      delh = 0
 endif
```